Exp. Anim. 55(1), 35–43, 2006

The Region-Specific Functions of Two Ubiquitin C-Terminal Hydrolase Isozymes along the Epididymis

Jungkee KWON[1, 3], Satoshi SEKIGUCHI[2], Yu-Lai WANG[1], Rieko SETSUIE[1], Yasuhiro YOSHIKAWA[2], and Keiji WADA[1]

[1]*Department of Degenerative Neurological Diseases, National Institute of Neuroscience, National Center of Neurology and Psychiatry, 4–1–1 Ogawahigashi, Kodaira, Tokyo 187-8502,*
[2]*Department of Biomedical Science, Graduate School of Agricultural and Life Sciences, The University of Tokyo, 1–1–1 Yayoi, Bunkyo-ku, Tokyo 113-8657, Japan, and*
[3]*Laboratory of Animal Medicine, College of Veterinary Medicine, Chonbuk National University, 664–14 Duckjin-Ku, Jeonju 561-756, Korea*

Abstract: *We previously showed that* gad *mice, which are deficient for ubiquitin C-terminal hydrolase L1 (UCH-L1), have a significantly increased number of defective spermatozoa, suggesting that UCH-L1 functions in sperm quality control during epididymal maturation. The epididymis is the site of spermatozoa maturation, transport and storage. Region-specific functions along the epididymis are essential for establishing the environment required for sperm maturation. We analyzed the region-specific expression of UCH-L1 and UCH-L3 along the epididymis, and also assessed the levels of ubiquitin, which has specificity for UCH-L1. In wild-type mice, western blot analysis demonstrated a high level of UCH-L1 expression in the caput epididymis, consistent with ubiquitin expression, whereas UCH-L3 expression was high in the cauda epididymis. We also investigated the function of UCH-L1 and UCH-L3 in epididymal apoptosis induced by efferent duct ligation. The caput epididymides of* gad *mice were resistant to apoptotic stress induced by efferent duct ligation, whereas* Uchl3 *knockout mice showed a marked increase in apoptotic cells following ligation. In conclusion, the response of* gad *and* Uchl3 *knockout mice to androgen withdrawal suggests a reciprocal function of the two UCH enzymes in the caput epididymis.*
Key words: *apoptosis, epididymis, ubiquitin, UCH*

Introduction

The mammalian epididymis is a highly convoluted tubule that connects the efferent ducts of the testis to the vas deferens [2, 8]. The epididymis is composed of three distinct compartments, caput (head), corpus (body) and cauda (tail), each having a specific role in sperm maturation, sustenance, transport, and storage [2, 6]. However, the molecular basis for the maturation process remains largely unknown.

It has been suggested that the epididymis acts as a quality control organ to eliminate defective spermato-

(Received 12 August 2005 / Accepted 4 November 2005)
Address corresponding: K. Wada, Department of Degenerative Neurological Diseases, National Institute of Neuroscience, National Center of Neurology and Psychiatry, 4–1–1 Ogawahigashi-cho, Kodaira, Tokyo 187-8502, Japan

zoa before ejaculation [37]. The epididymis is an organ with voluminous protein traffic between the epithelium and lumen. Numerous proteins, secreted in an apocrine manner by the epididymal epithelium, are implicated in spermatozoa maturation [18]. Two major components of the ubiquitin-dependent proteolytic pathway, ubiquitin and UCH-L1 (PGP9.5), are expressed in epididymal tissue [10, 35]. Ubiquitin is present in human seminal plasma [26], and defective spermatozoa become ubiquitinated during epididymal passage [23, 37]. Our previous work showed that UCH-L1 associates with monoubiquitin and stabilizes its expression [31]. In addition, it has been suggested that UCH-L1 functions as a regulator of apoptosis via the ubiquitin pathway [13, 23, 25]. We found that testes of gracile axonal dystrophy (*gad*) mice, which lack UCH-L1, have reduced ubiquitin levels and are resistant to cryptorchid injury–mediated germ cell apoptosis [25]. Furthermore, our recent work demonstrated that the percentage of morphologically abnormal spermatozoa is significantly higher in *gad* mice, compared with wild-type mice [23].

Two mouse UCH isozymes, UCH-L1 and UCH-L3, are strongly but reciprocally expressed in the testis during spermatogenesis [25], suggesting that these proteins have distinct functions in the testis [23], even though they have high amino acid sequence identity and share significant structural similarity [21]. The functional regionalization of the epididymis is delineated at the molecular level by regional differences in gene expression [16–19]. Regional differences along the epididymis might be essential characteristics of the environment required for sperm quality control. Although it has been shown that UCH-L1 and UCH-L3 have reciprocal functions with respect to cryptorchid injury, their molecular functions in regulating sperm quality during epididymal passage are not fully understood. Thus, we examined the epididymal expression of UCH-L1 and UCH-L3 with regard to their involvement in the regulation of apoptosis. In addition, we assessed the reciprocal functions of these two proteins in the epididymis.

Materials and Methods

Animals

We used *gad* (CBA/RFM) [34] and *Uchl3* knockout (C57BL/6J) [21] male mice at 10 weeks of age. The *gad* mouse is an autosomal recessive mutant that was obtained by crossing CBA and RFM mice. The *gad* line has been maintained by intercrossing for more than 20 generations [34]. *Uchl3* knockout mice were generated by the standard method [21] using homologously recombinant ES cells, and the knockout line has been back-crossed several times to C57BL/6J mice. Both strains are maintained at our institute. Animal care and handling were in accordance with our institutional regulations for animal care and were approved by the Animal Investigation Committee of the National Institute of Neuroscience, National Center of Neurology and Psychiatry.

Unilateral efferent duct ligation

Animals were either left intact to serve as controls or were unilaterally ligated at the efferent duct [9, 38]. Four mice in each group were anesthetized with pentobarbital (Abbott Laboratories, North Chicago, IL), and the testis and epididymis on the right side were exposed through a scrotal incision. The thin avascular attachment joining the initial segment of the epididymis to the tunica albuginea was cut to permit exposure of the efferent ducts coursing above and parallel to the vascular supply. A silk suture was passed by needle through the thin sheet of connective tissue between the ductules and the blood vessels, and the efferent ducts were occluded by ligation. Mice were sacrificed 2 or 4 days after ligation. Both epididymides were immersed in 4% paraformaldehyde for at least 24 hr before they were dehydrated and embedded in paraffin [22].

Histological and immunohistochemical assessment of the epididymis

The caput, corpus and cauda epididymides along the epididymal region embedded in paraffin were cut into 4-μm sections and stained with hematoxylin and eosin. Light microscopy was used for routine observations. For immunohistochemical staining, the sections were incubated with 10% goat serum for 1 h at room temperature followed by incubation overnight at 4°C with a rabbit polyclonal antibody raised against peptides within UCH-L1 or UCH-L3 (1:1,000 dilution; peptide antibodies [24]) and ubiquitin (1:500; DakoCytomation, Glostrup, Denmark) in PBS containing 1% BSA. Sections were then incubated for 1 h with biotin-conjugated anti-rabbit IgG diluted 1:200 in PBS, followed by

Vectorstain ABC-PO (Vector Laboratories, Burlingame, CA) for 30 min at room temperature. Sections were developed using 3,3'-diaminobenzidine and counterstained with hematoxylin.

In situ apoptosis was detected by TUNEL (TdT-mediated nick end-labeling) staining with the DeadEnd Fluorometric TUNEL system (Promega, Madison, WI) according to the manufacturer's instructions, to identify apoptotic cells in situ via specific labeling of nuclear DNA fragmentation. Quantification was performed using four mice on each of postoperative days 0, 2 and 4. The total number of apoptotic cells was determined by counting the positively stained nuclei in each caput epididymis section [9]. Four sections from each mouse and 100 total circular tubules per group were processed.

Western blotting

Western blots were performed as previously reported [24]. Total protein (10 μg/lane) from each epididymal region including spermatozoa was subjected to SDS-polyacrylamide gel electrophoresis using 15% gels (Perfect NT Gel, DRC, Japan). Proteins were electrophoretically transferred to polyvinylidene difluoride membranes (Bio-Rad, Hercules, CA) and blocked with 5% non-fat milk in TBS-T (50 mM Tris base, pH 7.5, 150 mM NaCl, 0.1% (w/v) Tween-20). The membranes were incubated individually with primary antibodies to monoubiquitin (1:1,000; u5379, Sigma-Aldrich, St. Louis, MO), UCH-L1 and UCH-L3 (1:1,000 dilution; anti-peptide antibodies [24]), p53, Bax, and Bcl-xL (1:1,000 dilution; all from Cell Signaling Technology, Beverly, MA), and Bcl-2 (1:500; Transduction Laboratories, Franklin Lakes, NJ). Blots were further incubated with peroxidase-conjugated goat anti-mouse IgG or goat anti-rabbit IgG (1:5,000 dilution; Pierce, Rockford, IL) for 1 h at room temperature. Immunoreactions were visualized using SuperSignal West Dura Extended Duration Substrate (Pierce) and analyzed using a ChemiImager (Alpha Innotech, San Leandro, CA). Each protein level was normalized to α-tubulin following analysis with a ChemiImager using AlphaEase software.

Statistical analysis

The mean and standard deviation were calculated for all data (presented as mean ± SD). Student's *t*-test was used for statistical analysis.

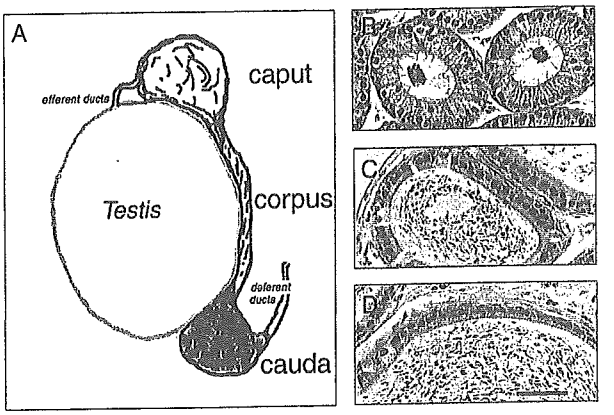

Fig. 1. A: Diagram of the epididymis. B–D: Morphology of the caput (B), corpus (C) and cauda (D) epididymidis from a wild-type mouse. Magnification, 200×. *Scale bar*, 40 μm.

Results

Levels of UCH-L1 and UCH-L3 in individual epididymal regions

The epididymis is a single long, coiled tubule situated on the surface of the testis (Fig. 1A). The epididymal epithelium is composed of four major cell types, principal cells, basal cells, clear cells and narrow cells [7], and can be divided anatomically and functionally into three regions, the caput, corpus and cauda epididymis (Fig. 1B, C, D). We used western blotting to characterize UCH-L1 and UCH-L3 levels along the epididymis (Fig. 2). In wild-type mice, the level of UCH-L1 was highest in the caput epididymis and that of UCH-L3 was highest in the cauda epididymis. UCH-L1 and UCH-L3 were not observed in *gad* and *Uchl3* knockout mice, respectively (Fig. 2; comparison of UCH-L1 and UCH-L3 levels with those in wild-type control mice).

Immunohistochemistry of UCH-L1, UCH-L3 and ubiquitin in the epididymis

Under light microscopy, granular and diffuse UCH-L1 and UCH-L3 immunoreactivity was detected in many epithelial cells of the caput, corpus and cauda epididymis in wild-type mice (Fig. 3A, C). Granular immunoreactivity to ubiquitin was seen in the epithelial cells of the epididymis (Fig. 3B). The distribution of ubiquitin in the corpus and cauda epididymal epithelial cells was similar to that of the caput epididymis,

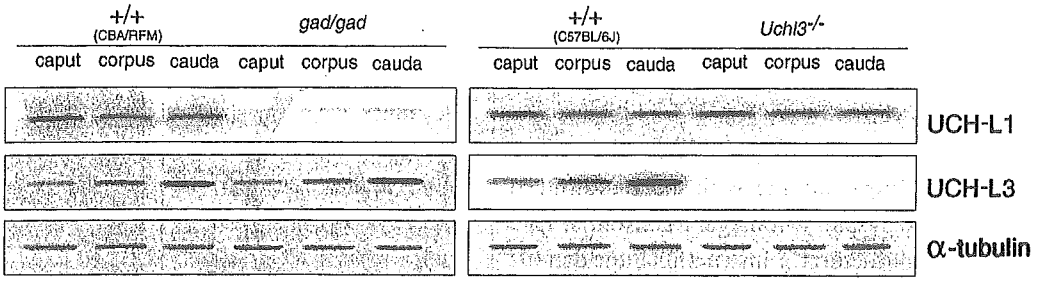

Fig. 2. Comparison of UCH-L1 and UCH-L3 expression by western blotting of caput, corpus and cauda epididymis lysates from two wild-type (CBA/RFM and C57BL/6J), *gad* and *Uchl3* knockout mice. Blots were reprobed for α-tubulin, which was used to normalize the protein load. Images are representative of four independent experiments.

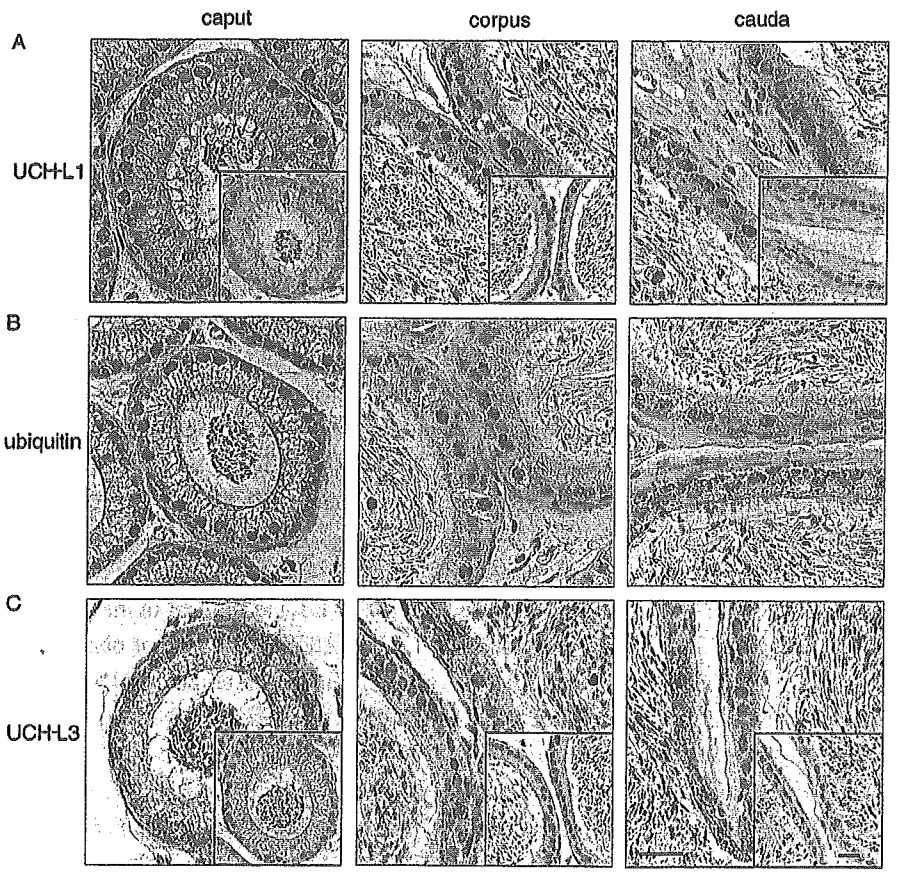

Fig. 3. Immunohistochemistry of UCH-L1, UCH-L3, and ubiquitin in the individual epididymal regions of wild-type mice. Each of the protein-positive cells in the caput, corpus and cauda epididymis is stained by DAB. The insets show that no cells are positive for UCH-L1 and UCH-L3 in the individual epididymal compartments from *gad* (A) and *Uchl3* knockout (C) mice, respectively. A: UCH-L1-positive cells. B: Ubiquitin-positive cells. C: UCH-L3-positive cells. Magnification, 400×. *Scale bar*, 20 μm.

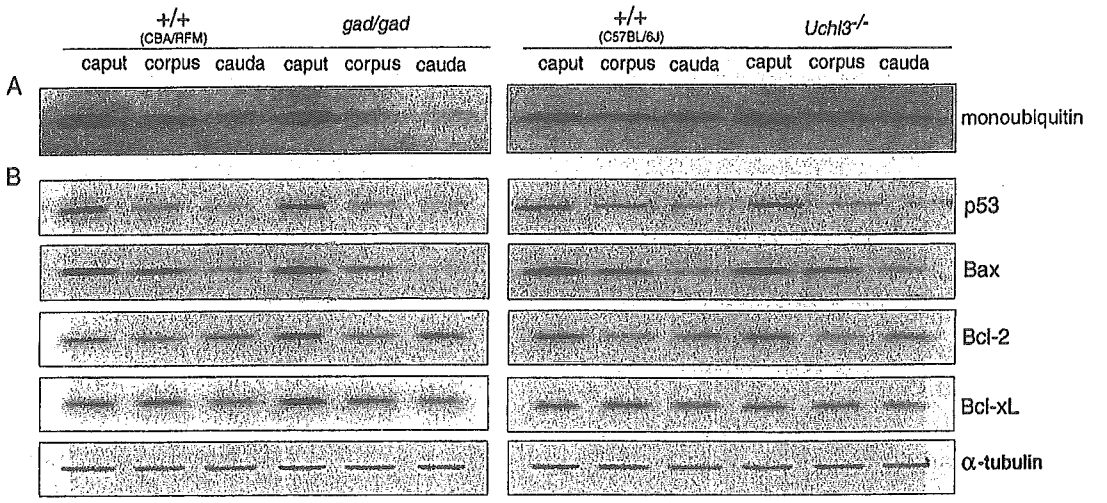

Fig. 4. Western blot analyses showing monoubiquitin and apoptotic proteins in the individual epididymal regions. Total protein (10 μg per lane) was prepared from the caput, corpus and cauda epididymidis from two wild-type (CBA/RFM and C57BL/6J), *gad* and *Uchl3* knockout mice. The blots show the expression levels of monoubiquitin (A) and apoptotic proteins (p53 and Bax) and antiapoptotic proteins (Bcl-2 and Bcl-xL) (B). Blots were reprobed for a-tubulin, which was used to normalize the protein load. Images are representative of four independent experiments.

the ubiquitin staining in these epididymal regions was less intense (Fig. 3B). Immunoreactivity to both UCH-L1 and ubiquitin was intense in the caput epididymal epithelial cells, which was consistent with the expression level (Fig. 2 and Fig. 4A). Diffuse cytoplasmic immunoreactivity in the epididymal epithelial cells to UCH-L3 was intense in the cauda epididymis (Fig. 3C). As shown previously [24], no UCH-L1 or UCH-L3 immunoreactivity was found in the epididymal epithelial cells of *gad* and *Uchl3* knockout mice, respectively (Fig. 3A, C. inset).

Region-specific localization of ubiquitin and apoptotic proteins in the caput epididymis

We previously reported that UCH-L1 binds ubiquitin, and that the level of ubiquitin is decreased in *gad* mice [25, 31]. To determine whether UCH-L1 is associated with the ubiquitin level in the epididymis, we performed western blot analysis of the individual epididymal regions. The monoubiquitin level was markedly higher in the caput epididymis than in the corpus and cauda epididymis, and the low level of monoubiquitin in *gad* mice is consistent with our previous report [25] (Fig. 4A). The epididymis of *Uchl3* knockout mice did not show a difference in ubiquitin level compared with the corresponding wild-type controls.

To explore whether apoptotic phenomenon of spermatozoa in the caput epididymis is in accord with the high expression of apoptotic proteins, we used western blot analysis to verify the expression levels of p53 and Bcl-2 family proteins, which are associated with cell death [12, 28, 29]. The levels of p53 and Bax protein, considered to be proapoptotic, were strikingly high in the caput epididymis, consistent with the pattern of the monoubiquitin level (Fig. 4B). In the *gad* mouse, the levels of the antiapoptotic proteins, Bcl-2 and Bcl-xL, were markedly elevated compared in wild-type mice in the caput epididymis [23] as well as a possible increase in the corpus and cauda epididymis, whereas the levels of apoptotic proteins, p53 and Bax, were unchanged (Fig. 4B). However, we did not detect a difference in the analyzed protein levels between the epididymis of *Uchl3* knockout and wild-type mice.

Region-specific apoptosis in the epididymis following unilateral efferent duct ligation

Androgen deprivation by efferent duct ligation induces glandular epithelial cell death via an apoptotic mechanism [9, 38]. We previously showed that germ cell apoptosis differs between *gad* and *Uchl3* knockout mice following cryptorchid injury [25]. To detect apoptosis in the epididymis following efferent duct li-

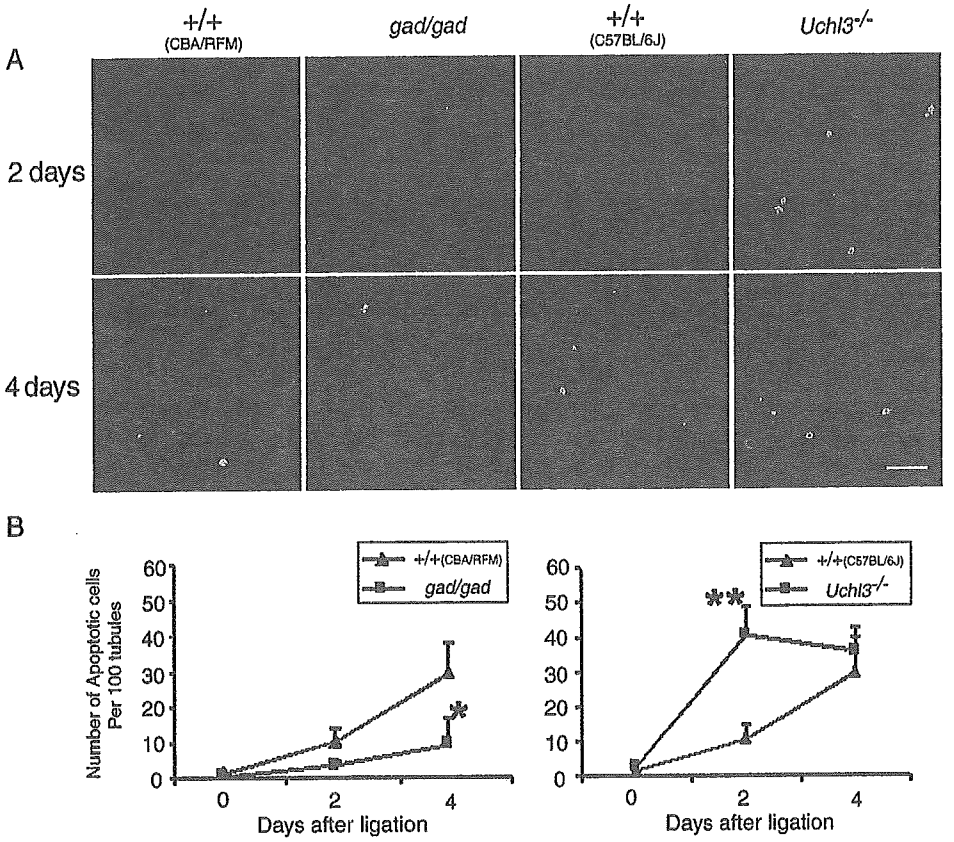

Fig. 5. TUNEL staining of apoptotic cells in the caput epididymis following unilateral efferent duct ligation. A: TUNEL staining in the caput epididymis cross-sections on days 2 and 4 after ligation. Green fluorescence, TUNEL-positive cells; red fluorescence, nuclei stained with propidium iodide. Magnification, 200×. *Scale bar*, 30 μm. B: Quantitation of epithelial cell apoptosis in the caput epididymis following efferent duct ligation. The number of apoptotic epithelial cells in *gad* and wild-type mice is shown on the left. Each value represents the mean ± SD; $^{*}P<0.05$. The number of apoptotic epithelial cells in *Uchl3* knockout and wild-type mice is shown on the right. Each value represents the mean ± SD; $^{**}P<0.01$.

gation, we used an *in situ* TUNEL assay to examine apoptosis in *gad* and *Uchl3* knockout mice on postoperative days 2 and 4 (Fig. 5). After efferent duct ligation, epithelial cell apoptosis was observed only in the caput epididymis (mostly the initial segment). The caput epididymis showed a time-dependent increase in epithelial cell apoptosis after efferent duct ligation and epithelial cell apoptosis was found mainly in the principal cells (Fig. 5A). Compared with wild-type mice, the caput epididymis of *Uchl3* knockout mice showed a marked increase in apoptotic epithelial cells on postoperative day 2, whereas *gad* mice resisted efferent duct-ligated epithelial cell apoptosis (Fig. 5A). By postoperative day 2, the number of apoptotic cells per 100 tubules increased with statistical significance ($^{**}P<0.01$, $n=4$) in the caput epididymis of *Uchl3* knockout mice as compared with wild-type mice (Fig. 5B). However, *gad* mice showed resistance to ligation-induced apoptosis in the caput epididymis relative to wild-type mice by postoperative day 4 ($^{*}P<0.05$, $n=4$) (Fig. 5B).

Discussion

After leaving the testis via the testicular rete, spermatozoa collect in the epididymis, where they undergo final maturation and storage [2, 36, 37]. During epididymal passage, ubiquitination may trigger apoptotic mechanisms that recognize and eliminate abnormal sper-

matozoa, and ubiquitination is believed to play an important role in controlling sperm quality to ensure the production of intact, functional spermatozoa [10, 27, 37]. Ubiquitination of abnormal spermatozoa predominantly occurs in the caput epididymis [37].

Previous studies have shown that two closely-related UCH isozymes, UCH-L1 and UCH-L3 have distinct expression patterns during spermatogenesis [24] and reciprocal functions following cryptorchid injury [25]. We have proposed that UCH-L1 might function as a regulator of apoptosis. Indeed, UCH-L1-deficient *gad* mice are resistant to apoptotic stress [13, 23, 25], and this apoptotic resistance leads to alterations in sperm motility and morphology as well as an increased number of defective spermatozoa in the epididymis of *gad* mice [23]. Our present study demonstrated that UCH-L1 and UCH-L3 have distinct expression patterns along the epididymis in wild-type mice (Fig. 2). We detected a high level of UCH-L1 in the caput epididymis, the main maturation organ, whereas the UCH-L3 level was high in the cauda epididymis, the main storage organ [10]. These region-specific variations in UCH-L1 and UCH-L3 level suggest that they have different functions in the epididymis. The regional differentiation of the epididymis, as suggested by region-specific gene expression, reflects different luminal environments between the regions [16, 19].

We also determined the expression pattern/level of the major component of the proteolytic pathway, ubiquitin, which has specificity for UCH-L1. UCH-L1 associates with monoubiquitin [31], and the monoubiquitin level is reduced in *gad* mice relative to wild-type mice [25, 31]. Predictably, monoubiquitin expression pattern showed similar patterns to UCH-L1 and the monoubiquitin level was reduced in the epididymis of *gad* mice, which had its highest level in the caput epididymis relative to the corpus or cauda epididymis in wild-type mice (Figs. 3 and 4A). Ubiquitin induction is important for regulating programmed cell death, which is a fundamental component of spermatogenesis [1, 23, 32]. Under specific circumstances, the caput epididymis contains a high level of ubiquitin, which may serve to maintain apoptotic mechanisms that eliminate abnormal spermatozoa [37]. This is consistent with the high levels of apoptotic p53 and Bax observed in the caput epididymis compared with the corpus and cauda epididymis (Fig. 4B). Protein p53 and Bax are classically thought to be involved in regulating apoptotic processes, and are targets for ubiquitination [5, 7, 29, 30]. The role of p53 in mediating apoptosis in the male genital tract has been demonstrated in several mice lines [28, 29, 42]. However, p53-independent apoptosis is suggested in the prostate and seminal vesicles by androgen withdrawal or in the rat epididymis by deprivation of luminal factors [3, 11, 14, 38]. Previous studies indicated that Bcl-2 family proteins are involved in the induction or prevention of apoptosis [12, 33, 39, 40]. In *gad* mice, in the present study, the levels of the antiapoptotic proteins, Bcl-2 and Bcl-xL, were markedly increased in the caput epididymis (Fig. 4B), although there was no difference in the levels of the apoptotic proteins, p53 and Bax, relative to wild-type mice. The high levels of Bcl-2 and Bcl-xL in the caput epididymis of *gad* mice is consistent with a previous report that the percentage of morphologically abnormal spermatozoa is significantly higher in *gad* mice [23]. Therefore, the variations of in the levels of Bax, and Bcl-2 and Bcl-xL combined in the caput epididymis probably maintain the regulation of apoptosis [4].

Our previous work focused on the reciprocal functions that UCH-L1 and UCH-L3 exhibit, a distinct feature in testicular germ cells following cryptorchid-induced apoptosis [25]. To characterize the distinct functions of UCH-L1 and UCH-L3 in the epididymis, *gad* and *Uchl3* knockout mice were examined after efferent duct ligation. The epididymal epithelium of the two mutant mice showed differences in apoptotic induction following efferent duct ligation (Fig. 5), after which the circulating androgen level decreases rapidly as a result of apoptotic cell death [9, 20, 38]. After duct ligation, the number of apoptotic cells increased in the caput epididymis of *Uchl3* knockout mice compared with wild-type mice, whereas *gad* mice showed relative resistance in this regard (Fig. 5B). In *gad* mice, the resistance to apoptotic stress can be explained by the high levels of Bcl-2 and Bcl-xL combined in the caput epididymis (Fig. 4B). The tissue androgen level is higher in the caput epididymis than in the corpus or cauda epididymis [15, 38]; thus, apoptotic cells showed in the caput epididymis rather than in the corpus and cauda epididymis following efferent duct ligation. These results may suggest that UCH-L1 and UCH-L3 have reciprocal functions in the caput epididymis fol-

lowing apoptotic stress induced by androgen withdrawal, as was shown with cryptorchid stress [25].

We cannot explain the profound apoptotic phenomenon observed in the present study in the caput epididymis of *Uchl3* knockout mice after efferent duct ligation by the balance of the Bcl-2 family proteins alone. Although our previous report showed that the Nedd8 expression level increased in the testis of *Uchl3* knockout mice [25], we found no difference in the present study (data not shown). The mechanism with regard to the antiapoptotic function of UCH-L3 requires further study. Our present study demonstrated that UCH-L1 and UCH-L3 have distinct expression levels along the epididymis as well as reciprocal functions in response to apoptotic stress induced by androgen withdrawal.

Acknowledgments

We thank H. Kikuchi for technical assistance with tissue sections, and M. Shikama for the care and breeding of animals.

Grant support: This work was supported by Grants-in-Aid for Scientific Research from the Ministry of Health, Labour and Welfare of Japan, Grants-in-Aid for Scientific Research from the Ministry of Education, Culture, Sports, Science and Technology of Japan, a grant from the Pharmaceuticals and Medical Devices Agency of Japan, and a grant from Japan Science and Technology Agency. This paper was supported (in part) by research funds of Chonbuk National University in 2005.

References

1. Baarends, W.M., van der Laan, R., and Grootegoed, J.A. 2000. Specific aspects of the ubiquitin system in spermatogenesis. *J. Endocrinol. Invest.* 23: 597–604.
2. Bedford, J.M. 1979. pp. 7–21. *In*: Evolution of the sperm maturation and sperm storage functions of the epididymis,The Spermatozoon (Bedford DWFaJM, ed). Urban and Schwarzenberg Inc., Baltimore-Muunich.
3. Berges, R.R., Furuya, Y., Remington, L., English, H.F., Jacks, T., and Isaacs, J.T. 1993. Cell proliferation, DNA repair, and p53 function are not required for programmed death of prostatic glandular cells induced by androgen ablation. *Proc. Natl. Acad. Sci. USA.* 90: 8910–8914.
4. Borner, C. 2003. The Bcl-2 protein family: sensors and checkpoints for life-or-death decisions. *Mol. Immunol.* 39: 615–647.
5. Chipuk, J.E. and Green, D.R. 2004. Cytoplasmic p53: Bax and Forward. *Cell Cycle* 3: 429–431.
6. Cooper, T.G. 1998. pp. 602–609. *In*: Epididymis, Encyclopedia of Reproduction (Neil EKaJD, ed). Academic Press Inc., San Diego.
7. Dimmeler, S., Breitschopf, K., Haendeler, J., and Zeiher, A.M. 1999. Dephosphorylation targets Bcl-2 for ubiquitin-dependent degradation: a link between the apoptosome and the proteasome pathway. *J. Exp. Med.* 189: 1815–1822.
8. Ezer, N. and Robaire, B. 2003. Gene expression is differentially regulated in the epididymis after orchidectomy. *Endocrinology* 144: 975–988.
9. Fan, X. and Robaire, B. 1998. Orchidectomy induces a wave of apoptotic cell death in the epididymis. *Endocrinology* 139: 2128–2136.
10. Fraile, B., Martin, R., De Miguel, M.P., Arenas, M.I., Bethencourt, F.R., Peinado, F., Paniagua, R., and Santamaria, L. 1996. Light and electron microscopic immunohistochemical localization of protein gene product 9.5 and ubiquitin immunoreactivities in the human epididymis and vas deferens. *Biol. Reprod.* 55: 291–297.
11. Furuya, Y., Lin, X.S., Walsh, J.C., Nelson, W.G., and Isaacs, J.T. 1995. Androgen ablation-induced programmed death of prostatic glandular cells does not involve recruitment into a defective cell cycle or p53 induction. *Endocrinology* 136: 1898–1906.
12. Gross, A., McDonnell, J.M., and Korsmeyer, S.J. 1999. BCL-2 family members and the mitochondria in apoptosis. *Genes. Dev.* 13: 1899–1911.
13. Harada, T., Harada, C., Wang, Y.L., Osaka, H., Amanai, K., Tanaka, K., Takizawa, S., Setsuie, R., Sakurai, M., Sato, Y., Noda, M., and Wada, K. 2004. Role of ubiquitin carboxy terminal hydrolase-L1 in neural cell apoptosis induced by ischemic retinal injury *in vivo*. *Am. J. Pathol.* 164: 59–64.
14. Jara, M., Esponda, P., and Carballada, R. 2002. Abdominal temperature induces region-specific p53-independent apoptosis in the cauda epididymidis of the mouse. *Biol. Reprod.* 67: 1189–1196.
15. Jean-Faucher, C., Berger, M., Gallon, C., de Turckheim, M., Veyssiere, G., and Jean, C. 1986. Regional differences in the testosterone to dihydrotestosterone ratio in the epididymis and vas deferens of adult mice. *J. Reprod. Fertil.* 76: 537–543.
16. Jervis, K.M. and Robaire, B. 2001. Dynamic changes in gene expression along the rat epididymis. *Biol. Reprod.* 65: 696–703.
17. Jervis, K.M. and Robaire, B. 2002. Changes in gene expression during aging in the Brown Norway rat epididymis. *Exp. Gerontol.* 37: 897–906.
18. Kirchhoff, C. 1998. Molecular characterization of epididymal proteins. *Rev. Reprod.* 3: 86–95.
19. Kirchhoff, C. 1999. Gene expression in the epididymis. *Int. Rev. Cytol.* 188: 133–202.
20. Knorr, D.W., Vanha-Perittula, T., and Lipsett, M.B. 1970. Structure and function of rat testis through pubescence. *Endocrinology* 86: 1298–1304.
21. Kurihara, L.J., Semenova, E., Levorse, J.M., and Tilghman,

S.M. 2000. Expression and functional analysis of Uch-L3 during mouse development. *Mol. Cell. Biol.* 20: 2498–2504.

22. Kwon, J., Kikuchi, T., Setsuie, R., Ishii, Y., Kyuwa, S., and Yoshikawa, Y. 2003. Characterization of the testis in congenitally ubiquitin carboxy-terminal hydrolase-1 (Uch-L1) defective (gad) mice. *Exp. Anim.* 52: 1–9.
23. Kwon, J., Mochida, K., Wang, Y. L., Sekiguchi, S., Sankai, T., Aoki, S., Ogura, A., Yoshikawa, Y., and Wada, K. 2005. Ubiquitin C-Terminal Hydrolase L-1 Is Essential for the Early Apoptotic Wave of Germinal Cells and for Sperm Quality Control During Spermatogenesis. *Biol. Reprod.* 73: 29–35.
24. Kwon, J., Wang, Y.L., Setsuie, R., Sekiguchi, S., Sakurai, M., Sato, Y., Lee, W.W, Ishii, Y., Kyuwa, S., Noda, M., Wada, K., and Yoshikawa, Y. 2004a. Developmental regulation of ubiquitin C-terminal hydrolase isozyme expression during spermatogenesis in mice. *Biol. Reprod.* 71: 515–521.
25. Kwon, J., Wang, Y.L., Setsuie, R., Sekiguchi, S., Sato, Y., Sakurai, M., Noda, M., Aoki, S., Yoshikawa, Y., and Wada, K. 2004b. Two closely related ubiquitin C-terminal hydrolase isozymes function as reciprocal modulators of germ cell apoptosis in cryptorchid testis. *Am. J. Pathol.* 165: 1367–1374.
26. Lippert, T.H., Seeger, H., Schieferstein, G., and Voelter, W. 1993. Immunoreactive ubiquitin in human seminal plasma. *J. Androl.* 14: 130–131.
27. Matin, R., Santamaria, L., Fraile, B., Paniagua, R., and Polak, J.M. 1995. Ultrastructural localization of PGP 9.5 and ubiquitin immunoreactivities in rat ductus epididymidis epithelium. *Histochem. J.* 27: 431–439.
28. Ohta, H., Aizawa, S., and Nishimune, Y. 2003. Functional analysis of the p53 gene in apoptosis induced by heat stress or loss of stem cell factor signaling in mouse male germ cells. *Biol. Reprod.* 68: 2249–2254.
29. Oren, M. 1999. Regulation of the p53 tumor suppressor protein. *J. Biol. Chem.* 274: 36031–36034.
30. Orlowski, R.Z. 1999. The role of the ubiquitin-proteasome pathway in apoptosis. *Cell Death Differ.* 6: 303–313.
31. Osaka, H., Wang, Y. L., Takada, K., Takizawa, S., Setsuie, R., Li, H., Sato, Y., Nishikawa, K., Sun, Y. J., Sakurai, M., Harada, T., Hara, Y., Kimura, I., Chiba, S., Namikawa, K., Kiyama, H., Noda, M., Aoki, S., and Wada, K. 2003. Ubiquitin carboxy-terminal hydrolase L1 binds to and stabilizes monoubiquitin in neuron. *Hum. Mol. Genet.* 12: 1945–1958.
32. Rasoulpour, R.J., Schoenfeld, H.A., Gray, D.A., and Boekelheide, K. 2003. Expression of a K48R mutant ubiquitin protects mouse testis from cryptorchid injury and aging. *Am. J. Pathol.* 163: 2595–2603.
33. Russell, L.D., Chiarini-Garcia, H., and Korsmeyer, S.J., Knudson, C.M. 2002. Bax-dependent spermatogonia apoptosis is required for testicular development and spermatogenesis. *Biol. Reprod.* 66: 950–958.
34. Saigoh, K., Wang, Y.L., Suh, J.G., Yamanishi, T., Sakai, Y., Kiyosawa, H., Harada, T., Ichihara, N., Wakana, S., Kikuchi, T., and Wada, K. 1999. Intragenic deletion in the gene encoding ubiquitin carboxy-terminal hydrolase in *gad* mice. *Nat. Genet.* 23: 47–51.
35. Santamaria, L., Martin, R., Paniagua, R., Fraile, B., Nistal, M., Terenghi, G., and Polak, J.M. 1993. Protein gene product 9.5 and ubiquitin immunoreactivities in rat epididymis epithelium. *Histochemistry* 100: 131–138.
36. Sutovsky, P. 2003. Ubiquitin-dependent proteolysis in mammalian spermatogenesis, fertilization, and sperm quality control: killing three birds with one stone. *Microsc. Res. Tech.* 61: 88–102.
37. Sutovsky, P., Moreno, R., Ramalho-Santos, J., Dominko, T., Thompson, W.E., and Schatten, G. 2001. A putative, ubiquitin-dependent mechanism for the recognition and elimination of defective spermatozoa in the mammalian epididymis. *J. Cell Sci.* 114: 1665–1675.
38. Turner, T.T. and Riley, T.A. 1999. p53 independent, region-specific epithelial apoptosis is induced in the rat epididymis by deprivation of luminal factors. *Mol. Reprod. Dev.* 53: 188–197.
39. Yamamoto, C.M., Sinha Hikim, A.P., Huynh, P.N., Shapiro, B., Lue, Y., Salameh, W.A., Wang, C., and Swerdloff, R.S. 2000. Redistribution of Bax is an early step in an apoptotic pathway leading to germ cell death in rats, triggered by mild testicular hyperthermia. *Biol. Reprod.* 63: 1683–1690.
40. Yang, E., Zha, J., Jockel, J., Boise, L.H., Thompson, C.B., and Korsmeyer, S.J. 1995. Bad, a heterodimeric partner for Bcl-XL and Bcl-2, displaces Bax and promotes cell death. *Cell* 80: 285–291.

doi:10.1093/brain/awh368 *Brain* (2005), **128**, 405–416

The slow Wallerian degeneration gene, *Wld*^{S}, inhibits axonal spheroid pathology in gracile axonal dystrophy mice

Weiqian Mi,[1,*] Bogdan Beirowski,[1,2,*] Thomas H. Gillingwater,[3] Robert Adalbert,[1,4] Diana Wagner,[1] Daniela Grumme,[1] Hitoshi Osaka,[5,6] Laura Conforti,[4] Stefan Arnhold,[2] Klaus Addicks,[2] Keiji Wada,[5] Richard R. Ribchester[3] and Michael P. Coleman[1,4]

[1]*ZMMK and Institute for Genetics and* [2]*Department of Anatomy I, University of Cologne, Cologne, Germany,* [3]*Division of Neuroscience, University of Edinburgh, Edinburgh,* [4]*The Babraham Institute, Babraham, Cambridge, UK,* [5]*Department of Degenerative Neurological Diseases, National Institute of Neuroscience, Kodaira, Tokyo and* [6]*Clinical Research Institute, Kanagawa Children's Medical Center, Yokohama, Japan*

Correspondence: Dr Michael Coleman, The Babraham Institute, Babraham, Cambridge CB2 4AT, UK
E-mail: michael.coleman@bbsrc.ac.uk
**W. Mi and B. Beirowski contributed equally to this work*

Summary

Axonal dystrophy is the hallmark of axon pathology in many neurodegenerative disorders of the CNS, including Alzheimer's disease, Parkinson's disease and stroke. Axons can also form larger swellings, or spheroids, as in multiple sclerosis and traumatic brain injury. Some spheroids are terminal endbulbs of axon stumps, but swellings may also occur on unbroken axons and their role in axon loss remains uncertain. Similarly, it is not known whether spheroids and axonal dystrophy in so many different CNS disorders arise by a common mechanism. These surprising gaps in current knowledge result largely from the lack of experimental methods to manipulate axon pathology. The slow Wallerian degeneration gene, *Wld*^{S}, delays Wallerian degeneration after injury, and also delays 'dying-back' in peripheral nervous system disorders, revealing a mechanistic link between two forms of axon degeneration traditionally considered distinct. We now report that *Wld*^{S} also inhibits axonal spheroid pathology in gracile axonal dystrophy (*gad*) mice. Both gracile nucleus ($P < 0.001$) and cervical gracile fascicle ($P = 0.001$) contained significantly fewer spheroids in *gad*/*Wld*^{S} mice, and secondary signs of axon pathology such as myelin loss were also reduced. Motor nerve terminals at neuromuscular junctions continued to degenerate in *gad*/*Wld*^{S} mice, consistent with previous observations that *Wld*^{S} has a weaker effect on synapses than on axons, and probably contributing to the fact that *Wld*^{S} did not alleviate *gad* symptoms. *Wld*^{S} acts downstream of the initial pathogenic events to block *gad* pathology, suggesting that its effect on axonal swelling need not be specific to this disease. We conclude that axon degeneration mechanisms are more closely related than previously thought and that a link exists in *gad* between spheroid pathology and Wallerian degeneration that could hold for other disorders.

Keywords: axon; axonal spheroid; gracile axonal dystrophy; ubiquitin; Wallerian degeneration

Abbreviations: APP = amyloid precursor protein; *gad* = gracile axonal dystrophy; GFAP = glial fibrillary acidic protein; H & E = haematoxylin and eosin; NMJ = neuromuscular junction; PFA = paraformaldehyde; PNS = peripheral nervous system; *Wld*^{S} = slow Wallerian degeneration gene, mutation or mice; Wld^S = slow Wallerian degeneration protein; YFP = yellow fluorescent protein

Received April 17, 2004. Revised August 12, 2004. Accepted November 1, 2004. Advance Access publication January 11, 2005

Introduction

Axonal dystrophy and spheroids are hallmarks of CNS axon pathology. Axonal spheroids are focal 10–50 μm diameter swellings, which are sometimes, but not always, terminal endbulbs, and are filled with disorganized neurofilaments,

tubules, organelles or multi-lamellar inclusions. Dystrophic axons are usually smaller swellings often associated with continuity of the axon. One or both of these aberrant axon morphologies is found in a wide range of CNS neurodegenerative disorders, including stroke (Dewar *et al.*, 1999), myelin disorders (Griffiths *et al.*, 1998), tauopathies (Lewis *et al.*, 2000; Probst *et al.*, 2000), amyotrophic lateral sclerosis (Tu *et al.*, 1996; Oosthuyse *et al.*, 2001; Howland *et al.*, 2002), traumatic brain injury (Cheng and Povlishock, 1988), Alzheimer's disease (Brendza *et al.*, 2003), Parkinson's disease (Galvin *et al.*, 1999), Creutzfeldt–Jakob disease (Liberski and Budka, 1999), HIV dementia (Raja *et al.*, 1997; Adle-Biassette *et al.*, 1999), hereditary spastic paraplegia (Ferreirinha *et al.*, 2004) and Niemann–Pick disease (Bu *et al.*, 2002). They also occur during normal ageing and secondarily in some serious illnesses (Sung *et al.*, 1981). In contrast, peripheral nervous system (PNS) axons undergo 'Wallerian-like' or 'dying-back' degeneration, even in diseases where CNS axons form swellings (Miura *et al.*, 1993; Lewis *et al.*, 2000; Oosthuyse *et al.*, 2001), although swellings do also occur in some rare PNS disorders (Miike *et al.*, 1986; Bomont *et al.*, 2000).

The roles of axonal swellings in disease are poorly understood, as illustrated by the following examples. First, in multiple sclerosis, many large spheroids are terminal endbulbs of transected axons but there are also a few 'en passant' swellings of similar shape and dimension (Trapp *et al.*, 1998) and many small dystrophic swellings (Ferguson *et al.*, 1997; Kornek *et al.*, 2000, 2001). It remains unclear whether these different types of swelling have common or different origins. Secondly, it is not clear whether disease-specific mechanisms lead to a common final pathway of axonal dystrophy, as in Alzheimer's disease, stroke and multiple sclerosis, and if so how they do this. Thirdly, it is not known why swellings predominate in distal axons in some diseases, such as gracile axonal dystrophy (*gad*) (Yamazaki *et al.*, 1988; Mukoyama *et al.*, 1989), caused by loss of ubiquitin C-terminal hydrolase l1 (*Uch-l1*) (Saigoh *et al.*, 1999), while in other diseases they occur in proximal axons, as in amyotrophic lateral sclerosis (Tu *et al.*, 1996) and tauopathy (Probst *et al.*, 2000). Finally, a better understanding is needed of the relationship between axon swelling and impaired axonal transport. Amyloid precursor protein (APP) accumulates in axonal swellings and spheroids in stroke (Dewar *et al.*, 1999), traumatic brain injury (Gentleman *et al.*, 1993), multiple sclerosis (Ferguson *et al.*, 1997), Creutzfeld–Jakob disease (Liberski and Budka, 1999), HIV dementia (Raja *et al.*, 1997; Adle-Biassette *et al.*, 1999) and *gad* (Ichihara *et al.*, 1995), indicating that axonal transport is impaired. However, it is not known whether axon swelling in these disorders is simply a consequence of impaired axonal transport, or whether it causes the transport defect, or both. These and other important questions remain unanswered largely because experimental methods to manipulate axonal swelling have not been available.

A mutant mouse gene, Wld^S, blocks a rate-limiting step common to Wallerian degeneration and diverse PNS axon disorders, including dysmyelination (Samsam *et al.*, 2003), motor neuronopathy (Ferri *et al.*, 2003) and Taxol toxicity (Wang *et al.*, 2002). Recently, Wld^S was reported to be effective in acute CNS lesions modelling stroke (Gillingwater *et al.*, 2004) and Parkinson's disease (Sajadi *et al.*, 2004) but its effect in a chronic CNS disease has not been reported. Wld^S is a chimeric gene (Conforti *et al.*, 2000) formed by a stable triplication (Coleman *et al.*, 1998; Mi *et al.*, 2003) encoding the N-terminus of multiubiquitylation factor Ube4b fused in-frame to nicotinamide mononucleotide adenylyltransferase (Nmnat1) plus a short novel sequence (Mack *et al.*, 2001). Nmnat1 appears to be sufficient to confer the phenotype *in vitro*, but it is not yet clear whether this holds *in vivo* (Coleman and Perry, 2002; Araki *et al.*, 2004). Wld^S protein appears to be restricted to the nucleus, so its effect on axons is mediated by other factors (Mack *et al.*, 2001), which may include the NAD-dependent deacetylase SIRT-1 (Araki *et al.*, 2004).

To study the relationship between axonal swelling and Wallerian degeneration, we crossed Wld^S and *gad* mice. Wld^S significantly reduced spheroid numbers without altering the first stages of *gad* pathogenesis, revealing a link between Wallerian degeneration and axonal spheroids in this disease that could extend to other disorders.

Methods

Origin, breeding and genotyping of mice

Homozygous C57BL/Wld^S spontaneous mutants were obtained from Harlan UK (Bicester, UK) and mated with heterozygous *gad* mice, kindly provided by Professor Keiji Wada and Dr Hitoshi Osaka (National Institute of Neuroscience, Tokyo, Japan), following a cross to C57BL/6 to ensure a more homogeneous genetic background. Thus, the genetic background of the experimental mice was 75% C57BL/6, 12.5% CBA/Nga, 12.5% RFM/Nga. Double heterozygotes were identified in the F1 generation by genotyping for *gad* (below) and intercrossed. *gad* homozygotes were identified by genotyping and selected for further study. Wld^S genotype was determined *post mortem* by pulsed-field gel electrophoresis of spleen DNA (Mi *et al.*, 2002). Hemizygous yellow fluorescent protein (YFP) mice of line YFP-H were obtained from Jackson Laboratories (Bar Harbor, MN, USA) and mated with *gad*/Wld^S double heterozygotes. Triple heterozygotes were then mated to *gad*/Wld^S double heterozygotes to produce *gad* homozygotes that were heterozygous for both Wld^S and YFP-H. For *gad* genotyping, tail genomic DNA was extracted at 3 weeks using the Nucleon II kit (Amersham Pharmacia), digested with *Pvu*II, and Southern blotted. It was then hybridized with a ^{32}P-labelled 764-bp probe generated by PCR from *gad* homozygous genomic DNA using primers 5′-ATCCAGGCGGCCCATGACTC-3′ and 5′-AGCTGCTTTGCAGAGAGCCA-3′. Positively hybridizing fragments indicative of the *gad* (0.75 kb) and wild-type (1.6 kb) alleles were then identified by autoradiography. To genotype for inheritance of the YFP-H transgene, the skin of a 1–2 mm ear punch at 21 days was pulled apart and fluorescent axons identified using a Zeiss Axiovert S100 inverted fluorescent microscope through the FITC filter.

Assessment of Wallerian degeneration

gad homozygotes that were heterozygous for *Wld*^{S} and hemizygous for the *YFP-H* transgene were anaesthetized prior to the onset of hindlimb weakness using intraperitoneal Ketanest (100 mg/kg; Parke Davis/Pfizer, Karlsruhe, Germany) and Rompun (5 mg/kg; Bayer, Leverkusen, Germany). The right sciatic nerve (upper thigh) was transected and the wound closed with a single suture. Five days later the mice were killed by cervical dislocation, the swollen first 2 mm of distal sciatic nerve was discarded and the next 2 mm was used for western blotting for heavy neurofilament protein as previously described (Mack *et al.*, 2001). The tibial nerve of the operated leg with a minimum of attached non-nervous tissue was processed for YFP fluorescence as follows. The nerve was stretched by ~10% by pinning onto a Sylgard (Du Pont) dish and fixed with 4% paraformaldehyde (PFA) (BDH Laboratory, UK) in 0.1 M phosphate-buffered saline (PBS) in the dark for 1 h. It was then incubated in 1% Triton X-100 (Sigma, Germany) in 0.1 M PBS for 10 min and washed three times with PBS before mounting in Vectashield (Vector Laboratories, USA). The degree of fragmentation of the representative subset of motor and sensory axons that are YFP-labelled was determined. For more detail, see Beirowski *et al.* (2004).

Preparation of gracile tract sections

Mice aged 126–130 days were anaesthetized using Ketanest and Rompun (100 mg/kg and 5 mg/kg intraperitoneally, respectively) or a higher dose as required for deep terminal anaesthesia. After sternotomy mice were killed by cardiac puncture and instantly intracardially perfused first with a solution containing 10 000 IE/l heparin (Liquemin N 25000; Hoffmann-La Roche) and 1% procainhydrochloride in 0.1 M PBS for 30 s and then with fixative (4% paraformaldehyde in 0.1 M PBS) for 10 min. Brain and spinal cord were carefully removed, further fixed in 4% PFA/0.1 M PBS overnight and extensively washed in 0.1 M PBS. Fixed tissues were extensively rinsed in fresh 0.1 M PBS, dehydrated in an ascending ethanol series and subsequently embedded in paraffin (Paraplast; Sherwood Medical Co., St Louis, MO, USA) applying standard histology techniques. Coronal serial sections (6 μm) were made using a Type HM355 microtome (Microm GmbH) from the entire gracile nucleus in medulla oblongata and cervical gracile fascicle starting at level 535 (Sidman *et al.*, 1971). Serial paraffin sections were mounted on conventional glass slides for use in haematoxylin and eosin (H & E) staining or on poly-L-lysine-coated slides for use in Luxol Fast Blue staining and immunocytochemistry, alternating normally every 2–3 sections. Distinction between gracile nucleus and cervical gracile fascicle was made by applying histomorphological criteria for the typical shapes of coronal sections.

H & E staining and spheroid quantification

Six-micrometre sections were deparaffinized in xylol (Carl-Roth, Germany) for 10 min, rehydrated in a descending ethanol series and rinsed in deionized H_2O for 1 min. Sections were placed in haematoxylin for 5 min, rinsed in tap water for 1 min to allow stain to develop and then placed in eosin for 2 min, dehydrated and mounted in Entellan resin (Merck, Germany). The occurrence of clearly detectable eosinophilic spheroids, indicative of dystrophic axons (Yamazaki *et al.*, 1988; Mukoyama *et al.*, 1989; Kikuchi *et al.*, 1990) was quantified in ~90 sections uniformly dispersed throughout the gracile nucleus of each individual and ~30 sections uniformly dispersed throughout the cervical gracile fascicle. Analysis of lateral columns was performed on these same 30 sections, counting the sum of spheroid numbers on both sides of the spinal cord. In this way, irregular results due to local deviations in spheroid numbers could be ruled out. H & E stained axonal spheroids were generally eosinophilic and appeared glassy or hyaline with a round or oval shape. They varied in diameter (5–50 μm) and sometimes reached a size larger than the nerve cells in gracile nucleus. All specimens were scored blind and agreed by two independent investigators.

Luxol Fast Blue staining and densitometric quantification

Six-micrometre sections from equivalent points in *gad* and *gad/Wld*^{S} cervical spinal cord and medulla oblongata were processed simultaneously as follows. Sections were deparaffinized in xylol (Carl-Roth, Germany) for 15 min, and processed twice through 100% ethanol for 2 min and 96% ethanol for a few seconds. Slides were transferred to Luxol Fast Blue solution [0.1% Luxol Fast Blue MBS chroma (Merck), 10% acetic acid all made up in 96% ethanol] and incubated at 60°C for 5 h. Sections were then rinsed in 95% ethanol and distilled water for 1 min each, dipped in 0.05% lithium carbonate (Merck) for 1 min, and differentiated in 70% ethanol for a further 1 min. After rinsing in distilled water, sections were examined under light microscope for suitable differentiation between white and grey matter. Nuclear Fast Red staining was carried out for 10 min in 5% aluminium sulphate, 0.1% Nuclear Fast Red followed by rinsing in distilled H_2O, 90% ethanol and 100% ethanol for 1 min each. Slides were incubated in xylol for 5 min and mounted in Entellan resin (Merck). Slides were examined under light microscopy (Nikon Eclipse E200) and evaluated using Bioscan OPTIMAS 6.0 software (Optimas Corp., WA, USA) according to the manufacturer's instructions. For densitometric quantitation, mean grey values were obtained for circumscribed areas of interest using a three-chip monochrome CCD camera, and the background grey value (tissue-free area) was subtracted. Since demyelination occurs selectively in the gracile tract and not in the cuneate tract of *gad* mice by 126–130 days (Mukoyama *et al.*, 1989; our observations), we used cuneate fascicle as a reference area and expressed Luxol Fast Blue staining in gracile tract as a percentage of that in cuneate tract. We applied this procedure to representative Luxol Fast Blue-stained sections of cranial gracile tract: two sections from level C2/C3 representing the cervical gracile fascicle and two sections from level 535 representing the gracile nucleus (Sidman *et al.*, 1971).

Immunocytochemistry of gracile tract

Six-micrometre paraffin sections from equivalent points in *gad* and *gad/Wld*^{S} cervical spinal cord and medulla oblongata were processed simultaneously as follows. Sections were deparaffinized, rehydrated in a descending ethanol series, washed several times in 0.05 M Tris-buffered saline (TBS), and treated with a solution of 6% H_2O_2 in methanol for 20 min to block endogenous peroxidase activity. They were then permeabilized with 0.1% Triton X-100 (Sigma) in 0.05 M TBS additionally containing 0.05 M NH_4Cl, rinsed in fresh TBS three times and subsequently immunoblocked with 5% bovine serum albumin (Sigma) in 0.05 M TBS

for 1 h. First antibody was polyclonal guinea pig anti-glial fibrillary acidic protein (GFAP) (1 : 400 dilution) (Progen, Germany) at 4°C overnight, while negative control sections were incubated without primary antibody. Secondary antibody was goat anti-guinea pig biotin conjugate (1 : 400 dilution) (Sigma) for 1 h at room temperature, and was followed by streptavidin-coupled horseradish peroxidase complex (Vector Laboratories; 1 : 200 dilution) for 1 h. After extensive washing, sections were developed under identical conditions for all specimens with 3,3-diaminobenzidine tetrahydrochloride (Sigma–Aldrich) in 0.1 M phosphate buffer until a clear dark-brown labelling of astrocytes in the gracile tract could be detected. In all cases the control sections without primary antibody incubation showed no labelling of astrocytes. For microscopic examination and TV densitometry, sections were dehydrated and mounted in Entellan resin (Merck). Quantitation was similar to that described for Luxol Fast Blue densitometry. GFAP immunostaining intensities in cranial gracile tract sections were expressed as percentage of GFAP staining intensity in wild-type sections at the same coronal level. We applied GFAP densitometry on representative cranial gracile tract sections from each examined mouse: two sections from level C2/C3 representing the cervical gracile fascicle and two sections from level 535 representing the gracile nucleus (Sidman *et al.*, 1971).

Immunocytochemistry of sciatic nerves

Sciatic nerves from 15-week-old *gad*, *gad*/*Wld*^{S}, or control mice were immersion fixed in 4% PFA/0.1 M PBS for 1 h and washed extensively in 0.1 M PBS before paraffin embedding. Twenty-micrometre sections were immunostained using rabbit polyclonal antibody to ubiquitin (Sigma–Aldrich U5379) and Cy3-conjugated secondary antibody. Confocal images were obtained using a PerkinElmer UltraView LCI confocal microscope coupled to a Nikon Eclipse TE200 microscope, and processed using UltraView software (Perkin-Elmer Life Sciences Ltd, Cambridge, UK).

Statistical analysis of histopathology results

All data (axonal spheroid numbers, TV densitometry intensities) are presented as mean ± SD for the examined genotype groups. Data analysis was performed using PRISM for Macintosh or SPSS for Windows, including Student's *t*-test calculations for paired and unpaired data where appropriate. Significance was considered at $P < 0.05$ and high significance at a $P < 0.01$.

Analysis of neuromuscular pathology

Mice were killed by cervical dislocation and lumbrical muscles immediately dissected under oxygenated Ringer solution. Fixation, immunocytochemistry and signal imaging were then carried out as described previously (Gillingwater *et al.*, 2002). The denervation rate was determined by counting 100–200 endplates in each of two to three lumbrical muscles and the mean value taken for each mouse.

Behavioural tests

The foot splay test (Norreel *et al.*, 2001) was used to estimate the reflex reaction speed of the hind limbs. Mice were gently taken by the neck and tail, the plantar surface of their hind feet painted using a non-toxic children's painting set, and the mouse released from a height of 15 cm to land on white paper. Wild-type mice bring their legs together during descent to land in a controlled manner like a gymnast, whereas *gad* mice fail to do this and land with their feet far apart. The distance between the two hind heels was averaged from 10 successive trials on each testing date (9 and 13 weeks).

In the clasping test, the mouse was suspended by the tail >50 cm from any surface. Clasping time within a 1 min test was scored as flexing or folding of the hind limbs tightly towards the trunk plus any spasmodic stretching. Mice were examined once per week through the period from 6 to 16 weeks. No wild-type mice clasped, regardless of the presence of the *Wld*^{S} mutation.

Results

gad does not weaken the Wld^S *phenotype*

Before assessing the effect of *Wld*^{S} on *gad* pathology we first showed that *Wld*^{S} can protect axons, even in the presence of the *gad* mutation, by inducing Wallerian degeneration in *gad*/*Wld*^{S} mice. Before the lesion, there was no sign of axon degeneration in these nerves, confirming previous reports (Mukoyama *et al.*, 1989). We bred *gad* mice that were heterozygous for *Wld*^{S} and hemizygous for a *YFP-H* transgene (Feng *et al.*, 2000) to allow a rapid and quantitative assessment of Wallerian degeneration (Beirowski *et al.*, 2004) and transected sciatic nerves before the onset of hindlimb weakness. Wallerian degeneration was assessed after 5 days both by western blotting to see degraded heavy neurofilament protein (Fig. 1A) and by fluorescence microscopy to see fragmented YFP-containing axons (Fig. 1B). Nerves unprotected by *Wld*^{S} degenerated as expected (Fig. 1A, middle lane, and Fig. 1B, lower panel) but a single allele of *Wld*^{S} was sufficient to prevent axon degeneration in both readout methods. Thus, *gad* does not significantly weaken the *Wld*^{S} phenotype and it is feasible to test the effect of *Wld*^{S} on *gad* pathology.

Axonal spheroid pathology is reduced by Wld^S

In order to determine the effectiveness of *Wld*^{S} on *gad* axonal spheroid pathology, we counted axonal spheroids in ~90 H & E stained 6-μm paraffin sections from throughout the gracile nucleus and 30 sections from throughout the cervical spinal cord of each 18-week-old *gad* mouse and *gad*/*Wld*^{S} double homozygote. Fifty per cent fewer spheroids were found in gracile nuclei of *gad*/*Wld*^{S} mice than in *gad* mice ($P = 0.0004$) and 63% fewer in cervical gracile fascicle ($P = 0.0011$) (Fig. 2). Intermediate values were observed in *Wld*^{S} heterozygotes, further supporting the result and no spheroids were observed in control animals of this age (data not shown). Spheroids have also been reported in the cervical lateral columns of *gad* mice (Kikuchi *et al.*, 1990). We found far fewer spheroids here than in cervical gracile tract and gracile nucleus, but the number was also significantly reduced by homozygous *Wld*^{S} ($P = 0.046$; $n = 3$) (Fig. 2). We also observed a reduction in axonal spheroids in lumbar spinal cord, from 42 to six in the ventral column and from 13 to four

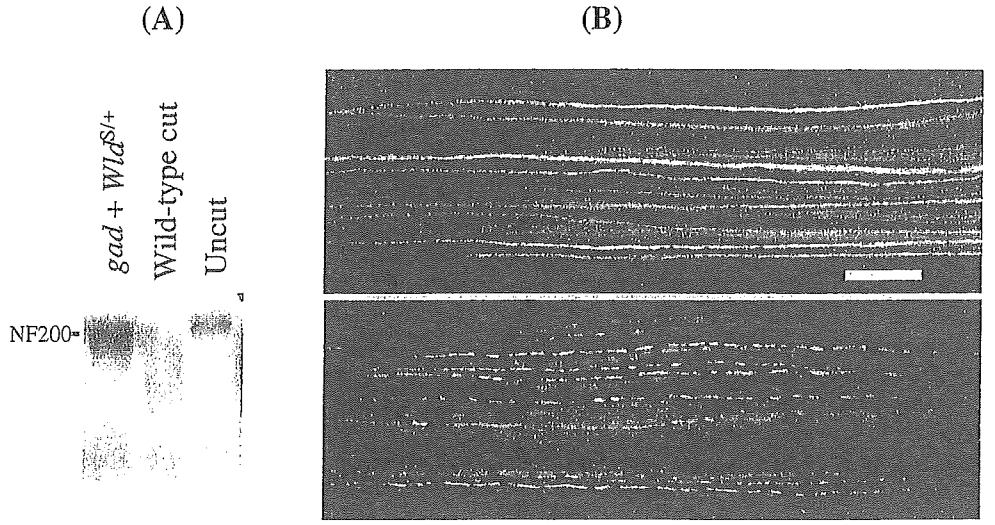

Fig. 1 A single allele of *Wld*^{S} is sufficient to delay Wallerian degeneration even in *gad* mice. (**A**) Western blot showing complete preservation of intact heavy neurofilament protein (NF200) in the distal stump of axotomized *gad* sciatic nerve by heterozygous *Wld*^{S} 5 days after lesion (lane 1). In contrast, no intact NF200 remains after 5 days in axotomized wild-type sciatic nerve (lane 2). Lane 3 is an uncut nerve showing the expected appearance of intact NF200 (gel loading differences probably account for the difference in intensity with lane 1). (**B**) Complete preservation of distal *gad* tibial nerve by heterozygous *Wld*^{S} 5 days after nerve lesion (upper panel), visualized using the *YFP-H* transgene. In contrast, no unfragmented axons remained in a tibial nerve lacking *Wld*^{S} 3 days after a lesion (lower panel). Unlesioned nerves appear exactly as in the upper image (Beirowski *et al.*, 2004). Scale bar = 100 μm.

in the dorsal horn grey matter. Although lumbar regions of only a single *gad* and two *gad/Wld*^{S} mice were studied, these mice were independent of those used for the gracile tract analysis and 3 weeks younger, so these data independently support our conclusion that *Wld*^{S} reduces axonal spheroid pathology in several different regions of *gad* CNS well into late-stage disease.

A reduction in the number of axonal spheroids could result theoretically from either reduced axon pathology or pathology so extensive that the axons are completely destroyed. Kurihara *et al.* (2001) reported that when *gad* pathology was made worse by crossing with *Uch-l3* null mice, extensive axon pathology became detectable at more caudal locations in cervical and thoracic gracile fascicle. We did not observe this in the *Wld*^{S} cross, and *Wld*^{S} homozygotes maintain a rostral–caudal gradient of axonal spheroid pathology (Fig. 2E and F; and thoracic data not shown), indicating that *gad* remains a 'dying-back' pathology in *Wld*^{S} mice but that its progress is delayed.

Secondary measures of axon pathology are also reduced by Wld^S

Further evidence of a reduced loss of axon-myelin units in *gad/Wld*^{S} mice came from a significant reduction ($P = 0.018$) in secondary myelin loss in cervical gracile fascicle in the same animals (Fig. 3A–C). A similar protective trend in the medulla oblongata did not reach statistical significance ($P = 0.059$), probably due to the naturally weaker myelination in this region, but *Wld*^{S} clearly did not cause any deterioration, so the reduction in axonal spheroid numbers (Fig. 2) must reflect reduced pathology and not wholesale axon loss. Furthermore, as the rescued axons remain myelinated, they potentially retain normal conductance properties, at least in these locations. It is unlikely that *Wld*^{S} has any direct effect on myelin, because expression of *Wld*^{S} in glia does not alter Wallerian degeneration (Glass *et al.*, 1993). Thus reduced myelin loss in *gad/Wld*^{S} mice is likely to reflect the maintenance of functional axon-myelin units. *Wld*^{S} also decreased GFAP signal in immunocytochemistry in *gad*, indicating a lower level of astrocyte activation in response to axon damage (Yamazaki *et al.*, 1988) (data not shown). Thus, both direct and indirect measures of spheroidal axon pathology in the gracile tract are reduced by the *Wld*^{S} gene.

Wld^S *operates downstream of axonal ubiquitin depletion in gad*

gad causes axon degeneration through defective ubiquitin metabolism (Osaka *et al.*, 2003), and *Wld*^{S} also interferes with ubiquitin metabolism (Mack *et al.*, 2001; Coleman and Perry, 2002; Zhai *et al.*, 2003). It was important to establish whether *Wld*^{S} blocks the ubiquitin defect in *gad*, an action that would suggest a protective effect restricted to *gad* and other ubiquitin defects, or whether it acts on a downstream step, raising the possibility of delaying axonal spheroid pathology in a wide range of CNS disorders (see above). Interpretation of any change in ubiquitin level in gracile tract would be complicated by the degeneration of those axon branches, so instead we carried out immunocytochemistry for ubiquitin epitopes in the peripheral branch of the same axons in sciatic nerve (Fig. 4). First, we confirmed that axonal ubiquitin was severely depleted in *gad* mice compared with wild-type controls ($P = 0.014$) (Osaka *et al.*, 2003). We then found

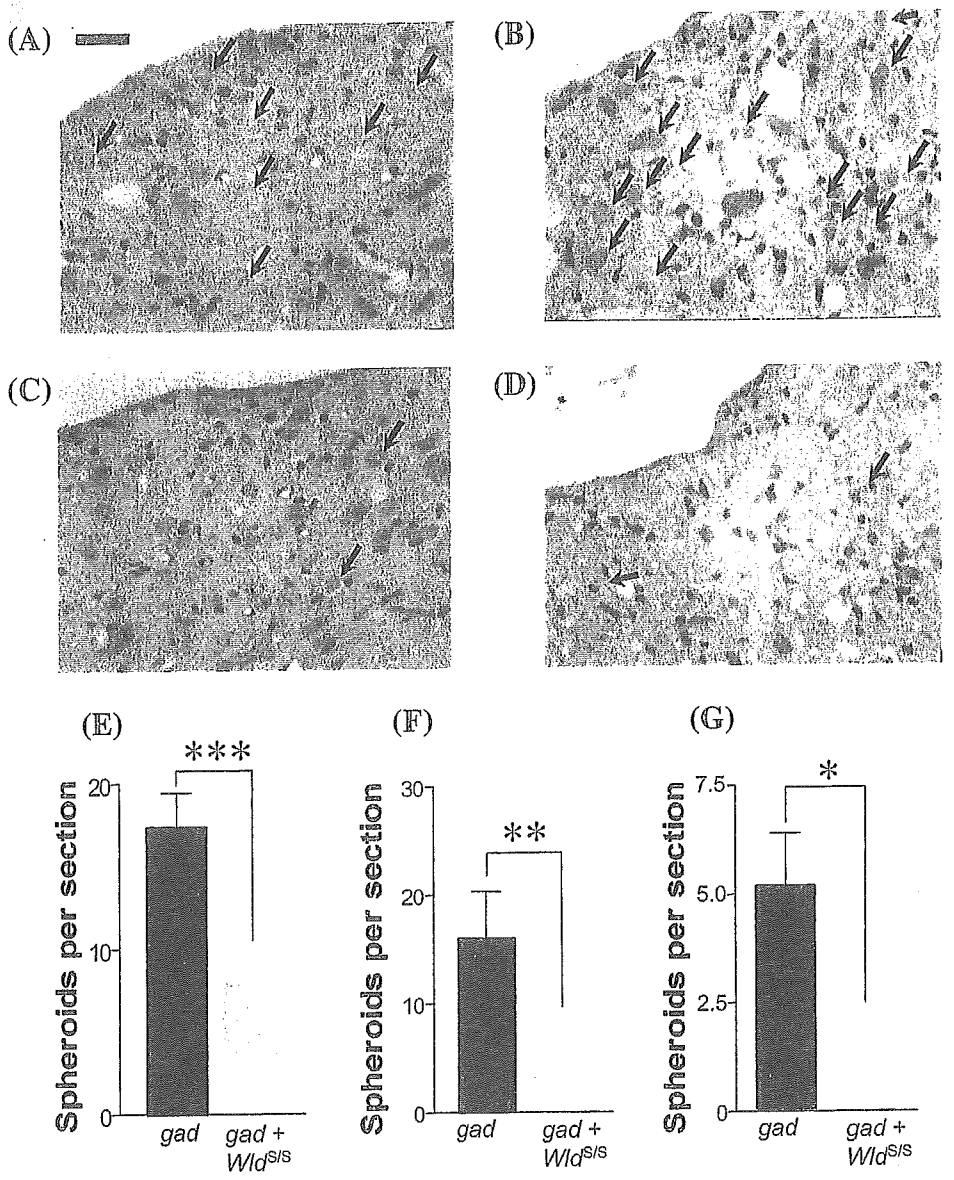

Fig. 2 *Wld*^{S} reduces spheroid body numbers in the gracile tract and lateral columns of *gad* mice. (**A** and **C**) Representative sections from gracile nucleus of (**A**) *gad* and (**C**) *gad/Wld*^{S} mice stained with H & E, showing a large reduction in the number of axonal spheroids (large pink swellings, indicated by arrows) when *Wld*^{S} is present. (**B** and **D**) Representative sections from cervical gracile fascicle of (**B**) *gad* and (**D**) *gad/Wld*^{S} mice. Scale bar (**A**–**D**) = 25 μm. (**E**–**G**) Quantitation (mean ± SD) of spheroid counting data in (**E**) gracile nucleus (n = 6), (**F**) cervical gracile fascicle (n = 6) and (**G**) cervical lateral columns (n = 3). *P < 0.05; **P < 0.01; ***P < 0.001.

that a similar defect was present in *gad/Wld*^{S} mice compared with *Wld*^{S} controls (P = 0.0004) and that *Wld*^{S} did not significantly increase the ubiquitin signal either in the presence (P = 0.902) or absence (P = 0.807) of *gad*. Thus, *Wld*^{S} does not correct the depletion of axonal ubiquitin in *gad* and instead operates at a downstream point in spheroid pathology that could be common to other CNS disorders.

Motor pathology

Despite the reduction in axonal spheroids in the gracile tract, there was no apparent reduction in the severity of *gad* symptoms when *Wld*^{S} was present, with no significant difference in hindlimb clasping, (P = 0.82; n = 9) or splay test (P = 0.33; n = 7). Thus, either prevention of swelling in the gracile tract does not preserve the function of those axons, or pathology elsewhere limits any improvement in phenotype of *gad/Wld*^{S} mice. In the absence of any tests to specifically target the function of gracile tract axons, we investigated neuromuscular junction (NMJ) pathology, where dying-back of motor nerve terminals has previously been reported (Miura *et al.*, 1993). At 15 weeks, the degree of denervation was similar between the two strains, with 56.0 ± 6.0% of lumbrical NMJ fully or partially denervated in *gad* mice and 53.5 ± 11.8% in *gad/Wld*^{S} (Fig. 5C and D). This may be because protection of motor nerve terminals at the NMJ by *Wld*^{S} after axotomy is weaker than that of the axon trunk, especially in older mice (Gillingwater *et al.*, 2002). However,

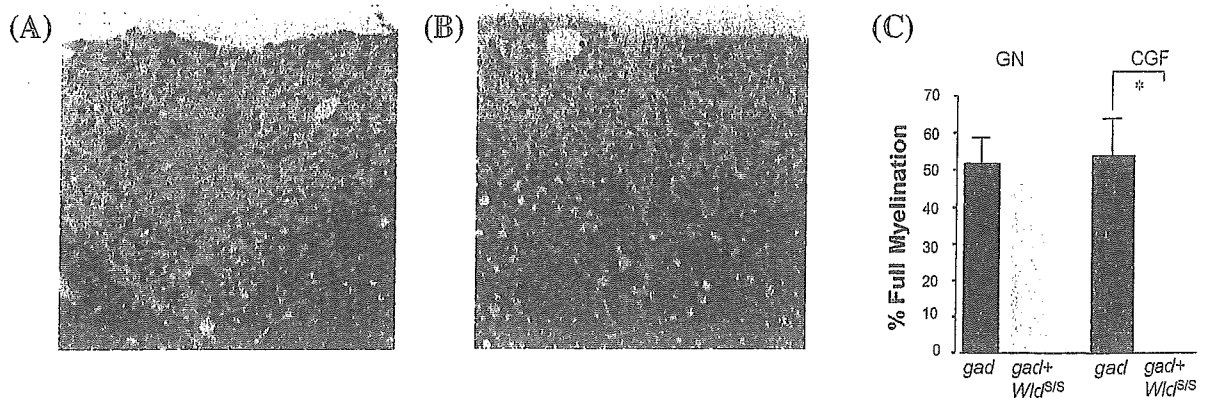

Fig. 3 *Wld*^{S} reduces also secondary demyelination in the gracile tract. (**A** and **B**) Representative cervical gracile fascicles of (**A**) *gad* and (**B**) *gad/Wld*^{S} mice stained with Luxol Fast Blue and Nuclear Fast Red, showing the reduction in myelin loss when *Wld*^{S} is present. Scale bar (**A** and **B**) = 25 μm. (**C**) Densitometric quantification (mean ± SD) of Luxol Fast Blue staining (n = 5). *P < 0.05.

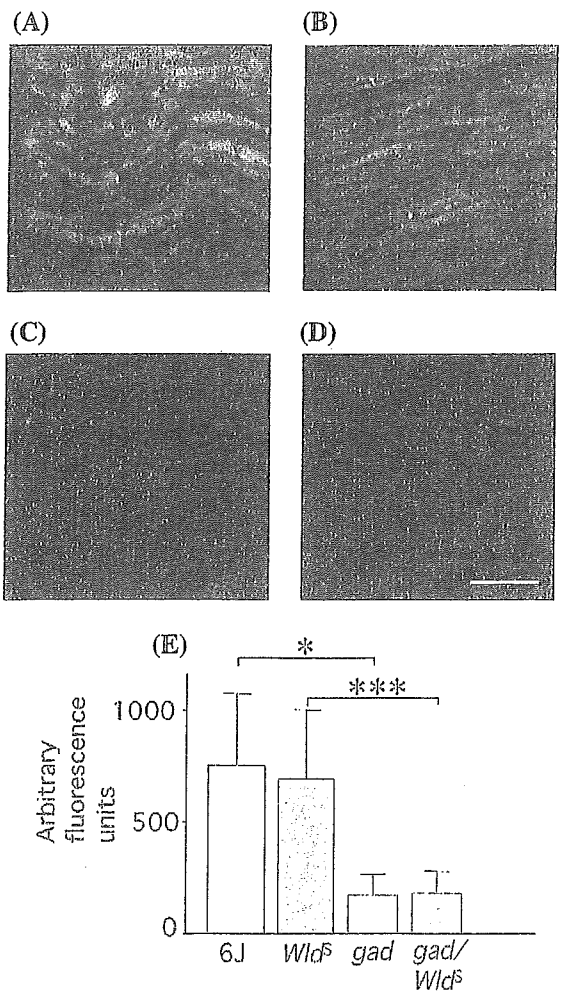

Fig. 4 *Wld*^{S} does not correct the severe depletion of axonal ubiquitin in *gad*. Ubiquitin immunostaining in both (**A**) wild-type and (**B**) *Wld*^{S} mice is greatly reduced in **C** and **D**, respectively, where *gad* is also present. Comparison of **A** with **B** and **C** with **D** also shows that *Wld*^{S} does not alter ubiquitin signal either in the presence of absence of *gad*. (**E**) Quantitation (mean ± SD) of ubiquitin signal. *P < 0.05; ***P < 0.001. 6 J, n = 4; *Wld*^{S}, n = 4; *gad*, n = 4; and *gad/Wld*^{S}, n = 10. Scale bar = 50 μm.

at 9 weeks, an age where *Wld*^{S} does protect axotomized motor nerve terminals, neither strain showed any denervation of NMJ in lumbrical muscles (Fig. 5A and B), so there was no time window when both *Wld*^{S} and *gad* exert their opposing effects at the NMJ. Thus, the fact that *Wld*^{S} does not alleviate NMJ pathology in the older mice could explain why *gad* symptoms are not reduced.

Discussion

We report that *Wld*^{S} reduces the occurrence of axonal spheroids in *gad*. This is the first indication that *Wld*^{S} can alleviate axon pathology in chronic CNS disease, thus extending observations made in the PNS that *Wld*^{S} protects axons not only after injury (Lunn *et al.*, 1989) but also in disorders where no physical injury takes place (Wang *et al.*, 2002; Ferri *et al.*, 2003; Samsam *et al.*, 2003). We conclude that axonal spheroid pathology in *gad* and Wallerian degeneration are not independent events and axon degeneration mechanisms are more uniform than morphology would suggest. It follows that Wallerian degeneration, or processes related to it, could contribute to many other CNS disorders where its involvement has not previously been suspected.

The mechanism by which *Wld*^{S} protects axons is still under investigation (Mack *et al.*, 2001; Coleman and Perry, 2002; Zhai *et al.*, 2003; Araki *et al.*, 2004), but appears to involve nuclear Wld^S protein and a factor(s) that communicates its effect to the axon. What is already becoming clear, however, is that *Wld*^{S} directly or indirectly blocks a central step of axon pathology onto which various pathological mechanisms converge (Fig. 6). This is indicated both by the wide range of disorders in which *Wld*^{S} protects axons, as it is inconceivable that *Wld*^{S} blocks different initial events in each case, and by our direct evidence, that early steps of *gad* pathogenesis are unaltered (Fig. 4). Intriguingly, it now seems that a number of different pathological manifestations result from the step delayed by *Wld*^{S}. These are axonal spheroids in *gad*, dying-back axon loss without swelling in peripheral

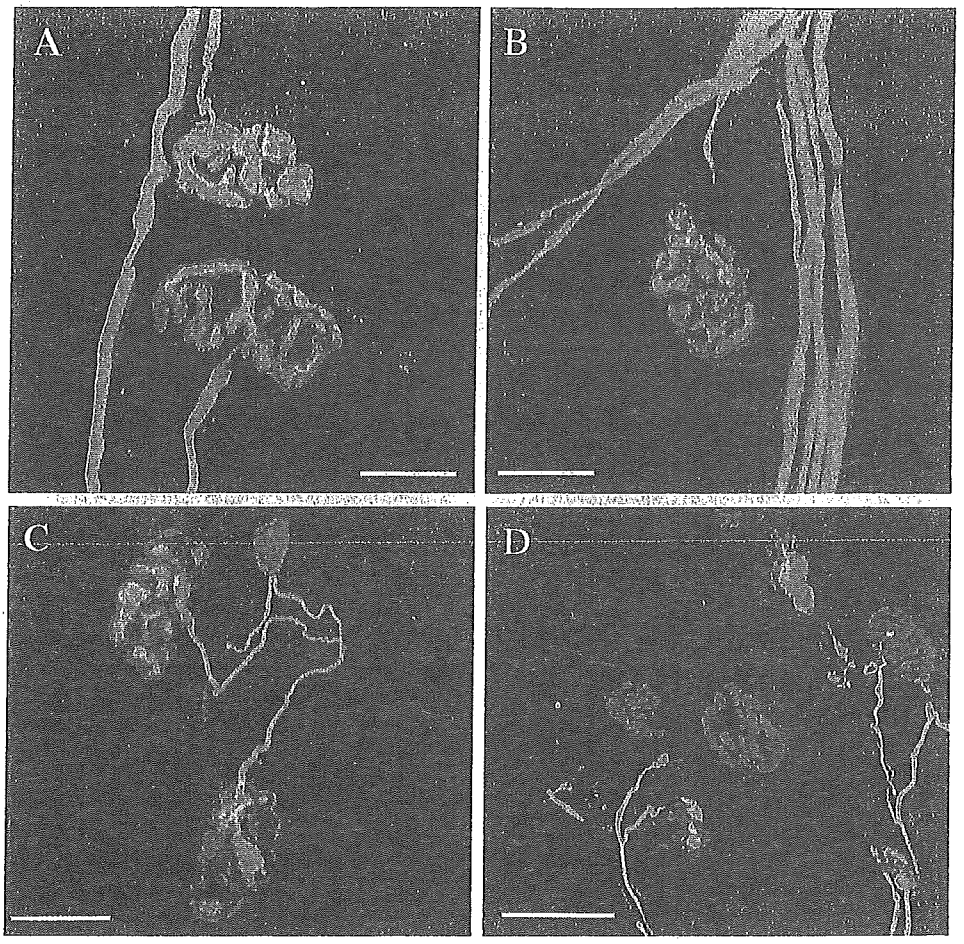

Fig. 5 Denervation at the NMJ. Presynaptic structures labelled with SV2 and neurofilament antibody are shown in green, and postsynaptic structures labelled with TRITC-α-bungarotoxin are in red. At 9 weeks, denervation has hardly begun in (**A**) *gad* or (**B**) *gad/Wld*^{S}. At 15 weeks, both strains show extensive denervation (**C** and **D**, respectively), with partial occupancy of endplates by motor nerve terminals occurring frequently. Scale bar = 25 μm.

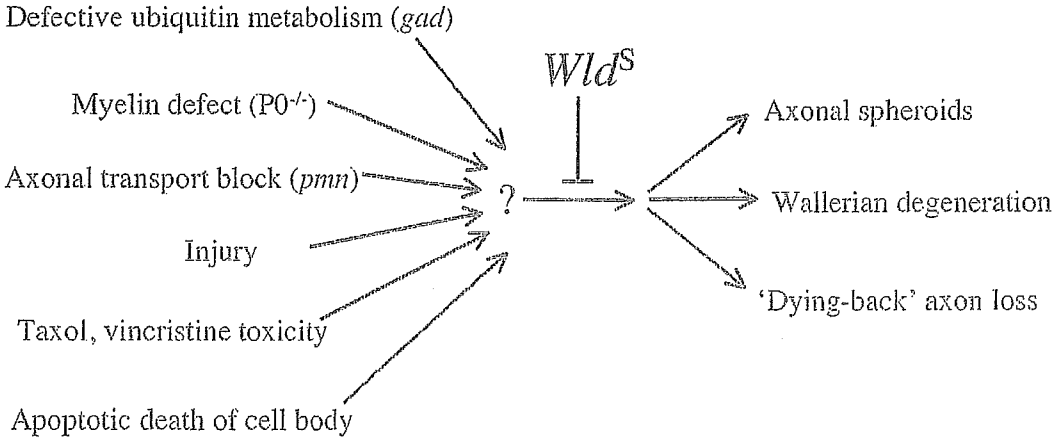

Fig. 6 *Wld*^{S} delays a central step of axonal pathology that lies after the convergence point of multiple degenerative stimuli but upstream of the divergence of several pathological manifestations.

neuropathy and motor neuronopathy, and Wallerian degeneration in CNS and PNS injury. The divergent morphology and topology in these disorders previously suggested independent mechanisms, but the results of directly probing the mechanism using *Wld*^{S} challenge this interpretation.

Many CNS disorders in which there is axonal swelling show accumulation of amyloid precursor protein in the swellings,

indicating impairment of axonal transport in each case and suggesting that their axon degeneration mechanisms are to some extent related. *gad* is one of these disorders, and the others include brain trauma (Gentleman *et al.*, 1993), stroke (Dewar *et al.*, 1999) and other forms of ischaemia (Hughes *et al.*, 2003), multiple sclerosis (Ferguson *et al.*, 1997), and HIV dementia (Medana and Esiri, 2003). This similarity with *gad* suggests that axon degeneration in other disorders may also be related to Wallerian degeneration, a possibility that should now be tested using Wld^S mice or, where appropriate, the newly generated Wld^S rat model (Adalbert *et al.*, in press). However, it is unlikely that Wld^S will stop all forms of axonal swelling, as it appears unable to do so in *Plp* null mice (Edgar *et al.*, 2004). Thus, it should be possible to categorize CNS axonal swelling disorders into those that are altered by Wld^S and those that are not. This will then enable disorders to be grouped together for mechanistic studies rather than focusing on each disorder in isolation.

It is important to consider the spatial and temporal relationship between axonal swelling and axonal breakdown in the light of our data. The lack of good methods for longitudinal imaging of CNS axons has made it difficult to determine whether spheroids first occur as terminal endbulbs of axons whose distal ends have degenerated, or as localized swellings on otherwise morphologically normal axons. Preliminary data from our laboratory using axons of *gad*/YFP-H mice (Adalbert and Coleman., unpublished) suggest that many spheroids in *gad* are not terminal endbulbs, at least in the early stages of the disease. Thus, one model to account for the effect of Wld^S in *gad* is that an 'en passant' spheroid is the first step in pathology, leading to degeneration of the distal axon due to the blockage of axonal transport, a process that fixes the spheroid as a terminal endbulb. In this model, Wld^S might block the Wallerian-like degeneration of the distal end for long enough to allow the spheroid to resolve and the axon to recover. Thus, our data suggest that Wld^S could be used to address the question of whether swollen axons can recover or whether they are destined, inevitably, to degenerate. In a wider context, this is an important issue in several CNS disorders where axonal spheroids occur, including brain trauma and multiple sclerosis (Cheng and Povlishock, 1988; Ferguson *et al.*, 1997).

The above model assumes that Wallerian-like degeneration and axonal swelling in *gad* are separated in space and time, with one causing the other. Alternatively, the mechanism of the axonal swelling itself in *gad* may be related to that of Wallerian degeneration. In support of this model, there are a number of disorders in which CNS axons swell and PNS axons of the same animal degenerate by Wallerian-like degeneration without extensive swelling. In *gad* mice, this occurs even within the same cell, as gracile tract central projections of lumbar primary sensory neurons have spheroids, while peripheral muscle spindles degenerate without swelling (Oda *et al.*, 1992). Similarly, amyotrophic lateral sclerosis (ALS) in humans (Tu *et al.*, 1996; Takahashi *et al.*, 1997), mice (Tu *et al.*, 1996; Oosthuyse *et al.*, 2001) and rats (Howland *et al.*, 2002), together with tauopathy in mice (Lewis *et al.*, 2000; Probst *et al.*, 2000), all show axonal swelling in spinal cord and other CNS areas, but extensive 'Wallerian-like' degeneration without swelling in ventral roots and peripheral nerves. Even injury-induced Wallerian degeneration shows different morphology depending on experimental circumstances. For example, when injured gracile tract axons undergo Wallerian degeneration they swell to up to 10 times their normal diameter, quite unlike Wallerian degeneration in the PNS (George and Griffin, 1994). Thus, a number of observations support a direct mechanistic link between axonal swelling and Wallerian degeneration.

It is not yet clear how related mechanisms might cause swelling in spheroids but axon fragmentation in Wallerian degeneration. Cytoskeletal changes are common to both, so a loosening of cytoskeletal structure could cause disorganized cytoskeleton to accumulate in spheroids but to undergo rapid granular disintegration in Wallerian degeneration. Wallerian degeneration of injured gracile tract axons displays elements of both processes, possibly having an intermediate mechanism: like spheroids, these axons dilate considerably but, typical of Wallerian degeneration, they also rapidly lose their cytoskeletal proteins (George and Griffin, 1994). In traumatic brain injury, observation of Wallerian degeneration and spheroids in the same transverse thin section has been interpreted as degenerating axons having a more proximal spheroid that blocks axonal transport (Cheng and Povlishock, 1988). In view of our findings, an additional explanation needs to be considered, that spheroids and Wallerian degeneration are alternative responses of different axons to the same lesion. Methods for real-time or long-range longitudinal analysis of individual spheroid-containing axons are required to resolve this, similar to new methods already applicable in PNS axons (Pan *et al.*, 2003; Beirowski *et al.*, 2004). What determines whether an axon develops a spheroid or undergoes Wallerian degeneration? Possible explanations include the different glial and haematopoietic cell content of the CNS and the lower rate of axonal transport there (Wujek and Lasek, 1983), but injury type may also be important. Finally, since the discovery of the Wld^S mouse, Wallerian degeneration is no longer considered a passive wasting of distal axons but a regulated self-destruction programme (Buckmaster *et al.*, 1995; Raff *et al.*, 2002). The reduction of axonal spheroid pathology in *gad* by the same gene raises similar questions: rather than being a passive consequence of blocked axonal transport axonal swelling could be, like Wallerian degeneration, a programmed response to axon damage.

Altered ubiquitin metabolism plays important roles in neurodegenerative diseases of the CNS. Genetic mutations in Parkinson's disease include an E3 ligase (Kitada *et al.*, 1998) and possibly *UCH-L1*, the human homologue of the gene mutated in *gad* (Leroy *et al.*, 1998). Ubiquitin-positive inclusions and other evidence indicate abnormal ubiquitylation in Alzheimer's disease (Mori *et al.*, 1987;

van Leeuwen *et al.*, 1998), polyglutamine disorders (DiFiglia *et al.*, 1997; Cummings *et al.*, 1999; Bence *et al.*, 2001) and ALS (Tu *et al.*, 1996; Bruijn *et al.*, 1997). Axons and synapses are particularly vulnerable, as proteasome inhibitors cause specific degeneration of distal neurites (Laser *et al.*, 2003) and ubiquitin-related mutations alter synapse growth (DiAntonio *et al.*, 2001) and stability (Wilson *et al.*, 2002). As Wld^S can counter a downstream effect of defective ubiquitin metabolism, it now becomes important to study its effects on the above disorders.

Wld^S did not alleviate the symptoms of *gad* mice. Unfortunately, methods do not currently exist to assess the function of gracile tract axons, so we cannot rule out the possibility that blocking spheroid formation did not preserve axon function. However, it is likely that continued neuromuscular pathology in *gad*/Wld^S mice also contributes to the symptoms. These mice suffered extensive synapse loss by 15 weeks (Fig. 5), whereas axon pathology was still strongly reduced 3 weeks later (Fig. 2). This supports the hypothesis that different mechanisms underlie synaptic and axonal degeneration, with Wld^S affording only limited protection to synapses, particularly in older mice (Gillingwater and Ribchester, 2001; Gillingwater *et al.*, 2002). Similarly, the synapses of gracile tract axons may have been lost even when those axons are preserved. Our data suggest that synapse pathology is a limiting factor when axons are protected by Wld^S, a finding likely to be important in other models (Ferri *et al.*, 2003; Samsam *et al.*, 2003).

In summary, we conclude that Wld^S alleviates chronic CNS axon pathology in *gad* mice and that formation of distal axonal spheroids in this disease shares features with Wallerian degeneration and 'dying-back' axon loss without spheroids. The effect of Wld^S on other CNS disorders with ubiquitylation deficits and CNS axonal swelling disorders should now be studied. Finally, our data emphasize the importance of finding a way to protect synapses as strongly as Wld^S protects axons.

Acknowledgements

We thank Professor Tateki Kikuchi for advice on *gad* pathology, Professor Rudolf Martini (University of Würzburg), Dr Mohtashem Samsam (University of Würzburg and Saba University School of Medicine), Dr Till G. A. Mack (Key Neurotek, Magdeburg, Germany), Dr Martin Bootman (The Babraham Institute, Cambridge) and Ms Jolanta Kozlowski (University of Cologne) for helpful discussion and technical advice. This work was supported by the Federal Ministry of Education and Research (FKZ: 01 KS 9502) and Center for Molecular Medicine, University of Cologne (CMMC) (to W.M., B.B., R.A., D.W., D.G. and M.P.C.), the Wellcome Trust (to T.H.G., plus Biomedical Collaboration Grant to R.R.R. and M.P.C), the Biotechnology and Biological Sciences Research Council (M.P.C., R.A., L.C.), ALSA (R.A.), the Koeln Fortune Programme (B.B.), the Grants-in-Aid for Scientific Research from the Ministry of Education, Culture, Sports, Science and Technology of Japan (K.W.) and from the Ministry of Health, Labour and Welfare of Japan (K.W.).

References

Adelbert R, Gillingwater TM, Haley JE, Bridge K, Beirowski B, Berek L, Wagner D, Grumme D, Thomson D, Celik A, Addicks K, Ribchester RR, and Coleman MP. A rat model of slow Wallerian degeneration (Wld^S) with improved preservation of synapses. Eur J Neurosci. In press.

Adle-Biassette H, Chretien F, Wingertsmann L, Hery C, Ereau T, Scaravilli F, et al. Neuronal apoptosis does not correlate with dementia in HIV infection but is related to microglial activation and axonal damage. Neuropathol Appl Neurobiol 1999; 25: 123–33.

Araki T, Sasaki Y, Milbrandt H. Increase nuclear NAD biosynthesis and SIRT1 activation prevent axonal degeneration. Science 2004; 305: 1010–3.

Beirowski B, Berek L, Adalbert R, Wagner D, Grumme DS, Addicks K, et al. Quantitative and qualitative analysis of Wallerian degeneration using restricted axonal labeling in YFP-H mice. J Neurosci Methods 2004; 134: 23–35.

Bence NF, Sampat RM, Kopito RR. Impairment of the ubiquitin–proteasome system by protein aggregation. Science 2001; 292: 1552–5.

Bomont P, Cavalier L, Blondeau F, Ben Hamida C, Belal S, Tazir M, et al. The gene encoding gigaxonin, a new member of the cytoskeletal BTB/kelch repeat family, is mutated in giant axonal neuropathy. Nat Genet 2000; 26: 370–4.

Brendza RP, O'Brien C, Simmons K, McKeel DW, Bales KR, Paul SM, et al. PDAPP;YFP double transgenic mice: a tool to study amyloid-b associated changes in axonal, dendritic and synaptic structures. J Comp Neurol 2003; 456: 375–83.

Bruijn LI, Becher MW, Lee MK, Anderson KL, Jenkins NA, Copeland NG, et al. ALS-linked SOD1 mutant G85R mediates damage to astrocytes and promotes rapidly progressive disease with SOD1-containing inclusions. Neuron 1997; 18: 327–38.

Bu B, Li J, Davies P, Vincent I. Deregulation of cdk5, hyperphosphorylation, and cytoskeletal pathology in the Niemann–Pick Type C murine model. J Neurosci 2002; 22: 6515–25.

Buckmaster EA, Perry VH, Brown MC. The rate of Wallerian degeneration in cultured neurons from wild type and C57BL/Wld^S mice depends on time in culture and may be extended in the presence of elevated K^+ levels. Eur J Neurosci 1995; 7: 1596–602.

Cheng CLY, Povlishock JT. The effect of traumatic brain injury on the visual system: a morphologic characterization of reactive axonal change. J Neurotrauma 1988; 5: 47–60.

Coleman MP, Perry VH. Axon pathology in neurological disease: a neglected therapeutic target. Trends Neurosci 2002; 25: 532–7.

Coleman MP, Conforti L, Buckmaster EA, Tarlton A, Ewing RM, Brown MC, et al. An 85-kb tandem triplication in the slow Wallerian degeneration (Wld^S) mouse. Proc Natl Acad Sci USA 1998; 95: 9985–90.

Conforti L, Tarlton A, Mack TG, Mi W, Buckmaster EA, Wagner D, et al. A Ufd2/D4Cole1e chimeric protein and overexpression of Rbp7 in the slow Wallerian degeneration (Wld^S) mouse. Proc Natl Acad Sci USA 2000; 97: 11377–82.

Cummings CJ, Reinstein E, Sun Y, Antalffy B, Jiang Y, Ciechanover A, et al. Mutation of the E6-AP ubiquitin ligase reduces nuclear inclusion frequency while accelerating polyglutamine-induced pathology in SCA1 mice. Neuron 1999; 24: 879–92.

Dewar D, Yam P, McCulloch J. Drug development for stroke: importance of protecting cerebral white matter. Eur J Pharmacol 1999; 375: 41–50.

DiAntonio A, Haghighi AP, Portman SL, Lee JD, Amaranto AM, Goodman CS. Ubiquitination-dependent mechanisms regulate synaptic growth and function. Nature 2001; 412: 449–52.

DiFiglia M, Sapp E, Chase KO, Davies SW, Bates GP, Vonsattel JP, et al. Aggregation of huntingtin in neuronal intranuclear inclusions and dystrophic neurites in brain. Science 1997; 277: 1990–3.

Edgar JM, McLaughlin M, Yool D, Zhang SC, Fowler JH, Montague P, et al. Oligodendroglial modulation of fast axonal transport in a mouse model of hereditary spastic paraplegia. J Cell Biol 2004; 166: 121–31.

Feng G, Mellor RH, Bernstein M, Keller-Peck C, Nguyen QT, Wallace M, et al. Imaging neuronal subsets in transgenic mice expressing multiple spectral variants of GFP. Neuron 2000; 28: 41–51.

Ferguson B, Matyszak MK, Esiri MM, Perry VH. Axonal damage in acute multiple sclerosis lesions. Brain 1997; 120: 393–9.

Ferreirinha F, Quattrini A, Pirozzi M, Valsecchi V, Dina G, Broccoli V, et al. Axonal degeneration in paraplegin-deficient mice is associated with abnormal mitochondria and impairment of axonal transport. J Clin Invest 2004; 113: 231–42.

Ferri A, Sanes JR, Coleman MP, Cunningham JM, Kato AC. Inhibiting axon degeneration and synapse loss attenuates apoptosis and disease progression in a mouse model of motoneuron disease. Curr Biol 2003; 13: 1–20.

Galvin JE, Uryu K, Lee VM, Trojanowski JQ. Axon pathology in Parkinson's disease and Lewy body dementia contains alpha-, beta-, and gamma-synuclein. Proc Natl Acad Sci USA 1999; 96: 13450–5.

Gentleman SM, Nash MJ, Sweeting CJ, Graham DI, Roberts GW. Beta-amyloid precursor protein (beta APP) as a marker for axonal injury after head injury. Neurosci Lett 1993; 160: 139–44.

George R, Griffin JW. The proximo-distal spread of axonal degeneration in the dorsal columns of the rat. J Neurocytol 1994; 23: 657–67.

Gillingwater TH, Ribchester RR. Compartmental neurodegeneration and synaptic plasticity in the Wld^S mutant mouse. J Physiol 2001; 534: 627–39.

Gillingwater TH, Thomson D, Mack TG, Soffin EM, Mattison RJ, Coleman MP, et al. Age-dependent synapse withdrawal at axotomised neuromuscular junctions in Wld^S mutant and Ube4b/Nmnat transgenic mice. J Physiol 2002; 543: 739–55.

Gillingwater TH, Haley JE, Ribchester RR, Horsburgh K. Neuroprotection after transient global cerebral ischemia in Wld(s) mutant mice. J Cereb Blood Flow Metab 2004; 24: 62–6.

Glass JD, Brushart TM, George EB, Griffin JW. Prolonged survival of transected nerve fibres in C57BL/Ola mice is an intrinsic characteristic of the axon. J Neurocytol 1993; 22: 311–21.

Griffiths I, Klugmann M, Anderson T, Yool D, Thomson C, Schwab MH, et al. Axonal swellings and degeneration in mice lacking the major proteolipid of myelin. Science 1998; 280: 1610–3.

Howland DS, Liu J, She Y, Goad B, Maragakis NJ, Kim B, et al. Focal loss of the glutamate transporter EAAT2 in a transgenic rat model of SOD1 mutant-mediated amyotrophic lateral sclerosis (ALS). Proc Natl Acad Sci USA 2002; 99: 1604–9.

Hughes PM, Anthony DC, Ruddin M, Botham MS, Rankine EL, Sablone M, et al. Focal lesions in the rat central nervous system induced by endothelin-1. J Neuropathol Exp Neurol 2003; 62: 1276–86.

Ichihara N, Wu J, Chui DH, Yamazaki K, Wakabayashi T, Kikuchi T. Axonal degeneration promotes abnormal accumulation of amyloid beta-protein in ascending gracile tract of gracile axonal dystrophy (GAD) mouse. Brain Res 1995; 695: 173–8.

Kikuchi T, Mukoyama M, Yamazaki K, Moriya H. Axonal degeneration of ascending sensory neurons in gracile axonal dystrophy mutant mouse. Acta Neuropathol (Berl) 1990; 80: 145–51.

Kitada T, Asakawa S, Hattori N, Matsumino H, Yamamura Y, Minoshima S, et al. Mutations in the parkin gene cause autosomal recessive juvenile parkinsonism. Nature 1998; 392: 605–8.

Kornek B, Storch MK, Weissert R, Wallstroem E, Stefferl A, Olsson T, et al. Multiple sclerosis and chronic autoimmune encephalomyelitis: a comparative quantitative study of axonal injury in active, inactive, and remyelinated lesions. Am J Pathol 2000; 157: 267–76.

Kornek B, Storch MK, Bauer J, Djamshidian A, Weissert R, Wallstroem E, et al. Distribution of a calcium channel subunit in dystrophic axons in multiple sclerosis and experimental autoimmune encephalomyelitis. Brain 2001; 124: 1114–24.

Kurihara LJ, Kikuchi T, Wada K, Tilghman SM. Loss of Uch-L1 and Uch-L3 leads to neurodegeneration, posterior paralysis and dysphagia. Hum Mol Genet 2001; 10: 1963–70.

Laser H, Mack TGA, Wagner D, Coleman MP. Proteasome inhibition arrests neurite outgrowth and causes 'dying-back' degeneration in primary culture. J Neurosci Res 2003; 15: 906–16.

Leroy E, Boyer R, Auburger G, Leube B, Ulm G, Mezey E, et al. The ubiquitin pathway in Parkinson's disease. Nature 1998; 395: 451–2.

Lewis J, McGowan E, Rockwood J, Melrose H, Nacharaju P, Van Slegtenhorst M, et al. Neurofibrillary tangles, amyotrophy and progressive motor disturbance in mice expressing mutant (P301L) tau protein. Nat Genet 2000; 25: 402–5.

Liberski PP, Budka H. Neuroaxonal pathology in Creutzfeldt–Jakob disease. Acta Neuropathol (Berl) 1999; 97: 329–34.

Lunn ER, Perry VH, Brown MC, Rosen H, Gordon S. Absence of Wallerian degeneration does not hinder regeneration in peripheral nerve. Eur J Neurosci 1989; 1: 27–33.

Mack TG, Reiner M, Beirowski B, Mi W, Emanuelli M, Wagner D, et al. Wallerian degeneration of injured axons and synapses is delayed by a Ube4b/Nmnat chimeric gene. Nat Neurosci 2001; 4: 1199–206.

Medana IM, Esiri MM. Axonal damage: a key predictor of outcome in human CNS diseases. Brain 2003; 126: 515–30.

Mi W, Conforti L, Coleman MP. Genotyping methods to detect a unique neuroprotective factor (Wld^S) for axons. J Neurosci Methods 2002; 113: 215–8.

Mi W, Glass JDG, Coleman MP. Stable inheritance of an 85-kb triplication in C57BL/Wld^S mice. Mut Res 2003; 526: 33–7.

Miike T, Ohtani Y, Nishiyama S, Matsuda I. Pathology of skeletal muscle and intramuscular nerves in infantile neuroaxonal dystrophy. Acta Neuropathol (Berl) 1986; 69: 117–23.

Miura H, Oda K, Endo C, Yamazaki K, Shibasaki H, Kikuchi T. Progressive degeneration of motor nerve terminals in gad mutant mouse with hereditary sensory axonopathy. Neuropathol Appl Neurobiol 1993; 19: 41–51.

Mori H, Kondo J, Ihara Y. Ubiquitin is a component of paired helical filaments in Alzheimer's disease. Science 1987; 235: 1641–4.

Mukoyama M, Yamazaki K, Kikuchi T, Tomita T. Neuropathology of gracile axonal dystrophy (gad) mouse. Acta Neuropathol 1989; 79: 294–9.

Norreel JC, Jamon M, Riviere G, Passage E, Fontes M, Clarac F. Behavioural profiling of a murine Charcot–Marie–Tooth disease type 1A model. Eur J Neurosci 2001; 13: 1625–34.

Oda K, Yamazaki K, Miura H, Shibasaki H, Kikuchi T. Dying back type axonal degeneration of sensory nerve terminals in muscle spindles of the gracile axonal dystrophy (gad) mutant mouse. Neuropathol Appl Neurobiol 1992; 18: 265–81.

Oosthuyse B, Moons L, Storkebaum E, Beck H, Nuyens D, Brusselmans K, et al. Deletion of the hypoxia-response element in the vascular endothelial growth factor promoter causes motor neuron degeneration. Nat Genet 2001; 28: 131–8.

Osaka H, Wang Y-L, Takada K, Takizawa S, Setsuie R, Li H, et al. Ubiquitin carboxy-terminal hydrolase L1 binds to and stabilises monoubiquitin in neurons. Hum Mol Genet 2003; 12: 1945–58.

Pan YA, Misgeld T, Lichtman JW, Sanes JR. Effects of neurotoxic and neuroprotective agents on peripheral nerve regeneration assayed by time-lapse imaging *in vivo*. J Neurosci 2003; 23: 11479–88.

Probst A, Gotz J, Wiederhold KH, Tolnay M, Mistl C, Jaton AL, et al. Axonopathy and amyotrophy in mice transgenic for human four-repeat tau protein. Acta Neuropathol (Berl) 2000; 99: 469–81.

Raff MC, Whitmore AV, Finn JT. Axonal self-destruction and neurodegeneration. Science 2002; 296: 868–71.

Raja F, Sherriff FE, Morris CS, Bridges LR, Esiri MM. Cerebral white matter damage in HIV infection demonstrated using beta-amyloid precursor protein immunoreactivity. Acta Neuropathol (Berl) 1997; 93: 184–9.

Saigoh K, Wang YL, Suh JG, Yamanishi T, Sakai Y, Kiyosawa H, et al. Intragenic deletion in the gene encoding ubiquitin carboxy-terminal hydrolase in gad mice. Nat Genet 1999; 23: 47–51.

Sajadi A, Schneider BL, Aebischer P. Wld^S-mediated protection of dopaminergic fibers in an animal model of Parkinson disease. Curr Biol 2004; 14: 326–30.

Samsam M, Mi W, Wessig C, Zielasek J, Toyka KV, Coleman MP, et al. The Wld^S mutation delays robust loss of motor and sensory axons in a